Co-targeting myelin inhibitors and CSPGs enhances sensory axon regeneration within, but not into, the spinal cord

Jinbin Zhai, Hyukmin Kim, Seung Baek Han, Meredith Manire, Rachel Yoo, Shuhuan Pang, George M. Smith and Young-Jin Son*

Shriners Hospitals Pediatric Research Center and Center for Neural Repair and Rehabilitation, Lewis Katz School of Medicine, Temple University, Philadelphia, PA 19140

* Corresponding author: Young-Jin Son, PhD
Tel: (215) 926-9354
Email: yson@temple.edu

ABSTRACT

A major barrier to intraspinal regeneration after dorsal root (DR) injury is the DR entry zone (DREZ), the CNS/PNS interface. DR axons stop regenerating at the DREZ, even if regenerative capacity is increased by a conditioning lesion. This potent blockade has long been attributed to myelin-associated inhibitors and CSPGs, but incomplete lesions and conflicting reports have hampered conclusive agreement. Here we evaluated DR regeneration in adult mice, using novel strategies to facilitate complete lesions and comprehensive analyses, selective tracing of proprio-/mechanoreceptive axons with AAV2, and genetic or viral targeting of Nogo, MAG, OMgp, CSPGs and GDNF. Simultaneously eliminating Nogo/MAG/OMgp elicited little intraspinal penetration of DR axons, even with additional removal of CSPGs and a conditioning lesion. Their absence, however, synergistically enhanced GDNF-elicited intraspinal regeneration. We conclude that myelin inhibitors and CSPGs constrain intraspinal regrowth of DR axons, but that they are not the primary mechanism(s) stopping axons at the DREZ.

INTRODUCTION

The dorsal root (DR) carries primary sensory axons that project centrally from dorsal root ganglion (DRG) neurons to secondary neurons within the spinal cord and brainstem. DR injuries commonly result from brachial plexus, lumbosacral plexus and cauda equina trauma, and may cause permanent loss of sensation, uncoordinated movement and chronic pain (Carlstedt, 2008; Kaiser et al., 2020). The devastating consequences are because DR axons stop regenerating at the entrance of the spinal cord, the dorsal root entry zone (DREZ), and thus fail to restore connections with secondary neurons. Animal studies have reported functional recovery of nociception (Ramer et al., 2000; Cafferty et al., 2007; Liu et al., 2009; Lin et al., 2014; Kelamangalath et al., 2015), and, less frequently, of proprioception and mechanoreception (e.g., Wang et al., 2008; Cheah et al., 2016), for which large-diameter, myelinated axons must regenerate far longer distances after crossing the DREZ.

Both neuron-intrinsic and extrinsic inhibitors, which limit axon regrowth elsewhere in the injured CNS (O'Shea et al., 2017; Griffin and Bradke, 2020), are widely thought to block regeneration at the DREZ. Notably, however, unlike direct CNS injury, DR injury damages axons peripherally in the PNS without causing an impassable glial scar. Nevertheless, DR axons

regenerating along the root quickly stop at the scar-free DREZ, even after a nerve conditioning lesion (Chong et al., 1999; Zhang et al., 2007; Di Maio et al., 2011). This potent blockade is surprising because a nerve conditioning lesion sufficiently enhances the growth potential of DRG neurons to penetrate a glial scar after spinal cord injury (Neumann and Woolf, 1999; Kwon et al., 2015). Why the scar-free DREZ is impenetrable even to conditioned axons remains unclear, but myelin-associated inhibitors and extracellular matrix-associated chondroitin sulfate proteoglycans (CSPGs) are conventionally considered responsible (Smith et al., 2012; Mar et al., 2016). Consistent with this notion, soluble peptides blocking interactions between myelin inhibitors and Nogo receptors are reported to dramatically enhance robust functional regeneration of myelinated, but not non-myelinated, axons after DR crush (Harvey et al., 2009; Peng et al., 2010). Similarly, blocking PTPσ, a CSPG receptor, is reported to produce functional regeneration of myelinated DR axons into the spinal cord (Yao et al., 2019). Activating integrins has been found to elicit long-distance, topographic and functional regeneration of both myelinated and unmyelinated DR axons, presumably by counteracting myelin inhibitors, CSPGs and tenascin-C (Tan et al., 2011; Cheah et al., 2016).

At least some of these observations have not been reproducible (Kelamangalath et al., 2015), and conflicting studies have reported that removing CSPGs alone enables only minimal penetration of DR axons through the DREZ (Steinmetz et al., 2005; Wu et al., 2016). CSPG removal, however, when combined with conditioning lesions, neurotrophic factors or inflammation, has significantly enhanced intraspinal regeneration of DR axons (Steinmetz et al., 2005; Wu et al., 2016; Guo et al., 2019). These reports have supported a major inhibitory role of CSPGs by suggesting that removing CSPGs alone only modestly increases regeneration presumably because myelin inhibitors are sufficient to stop axons at the DREZ.

Despite the long-held view attributing the potent blockade to myelin inhibitors and CSPGs, whether they indeed are primarily responsible for the regeneration failure at the DREZ has not been determined. It is also unknown whether they are equally potent and act synergistically. Also undetermined is whether their removal promotes regeneration of DR axons within the spinal cord in addition to across the DREZ and how robustly unconditioned or conditioned DR axons regenerate in the absence of both myelin inhibitors and CSPGs.

The present studies address these questions and attempt to determine the roles of myelin inhibitors and CSPGs at the DREZ and within the spinal cord. We selectively traced regenerating proprioceptive and mechanoreceptive axons and used a novel wholemount assay to ensure that DR lesions were complete and the analysis comprehensive. We found that DR axons rarely penetrate the DREZ, even after supplementary removal of CSPGs and addition of a conditioning lesion, in triple knockout (tKO) mice lacking major myelin inhibitors-Nogo (A, B, C), MAG and OMgp. Their absence, however, synergistically enhances intraspinal regeneration of DR axons elicited by GDNF. Thus, myelin inhibitors and CSPGs are not crucial factors blocking sensory axons at the DREZ, although they synergistically constrain regrowth of DR axons within the spinal cord. These findings substantially advance current understanding of sensory axon regeneration across the CNS/PNS border.

RESULTS

Intraganglionic AAV2-GFP selectively labels proprioceptive and mechanoreceptive axons

Conventional assessment of DR regeneration has relied heavily on immunolabeling of tissue sections and consequently was subject to labeling artifacts and limited sensitivity. We initiated the present study by identifying a viral tracer that intensely and reliably labels regenerating DR axons. We tested various recombinant viral vectors carrying fluorescent reporters by microinjecting them into cervical DRGs of uninjured adult mice. Of those we examined at 2 weeks post-injection, AAV2-GFP (self-complementary adeno-associated virus serotype 2-enhanced green fluorescent protein) almost exclusively transduced neurons, revealing brightly labeled cell bodies and axons (Figure 1A). After optimizing the virus titer, dosage and microinjection technique, we were able to infect >70% neurons in most injections of DRGs (Figure 1B). Infected neurons included the three broadly classified subtypes of DRG neurons: large, neurofilament (NF)+ neurons, small- and medium sized IB4+ non-peptidergic neurons and small CGRP+ peptidergic neurons (Figure 1C). Notably, a majority of the transduced, GFP-expressing neurons were NF+ (Figure 1D). In contrast, IB4+ neurons rarely were GFP+ and ~30% of GFP+ neurons were CGRP+ (Figure 1D), indicating that NF+ neurons were disproportionately transduced by AAV2-GFP. Consistent with the preferential infection of NF+ neurons, brightly labeled, large-diameter axons projected into the deeper layers of the dorsal

horn (layer III-V) and into ventral horn, where large myelinated axons terminate (Figure 1E). In contrast, superficial laminae of the dorsal horn, where small diameter unmyelinated axons terminate (layer I, II), lacked GFP fluorescence (Figure 1E' and E"), showing that AAV-GFP labels few if any IB4+ and CGRP+ axons. These findings demonstrate that AAV2-GFP predominantly transduces NF+ neurons and selectively reveals their axons within the spinal cord.

NF+ neurons extend large-diameter myelinated axons that relay proprioception or mechanoreception via second order neurons located deep in the spinal cord and in distant dorsal column nuclei in the medulla (Niu et al., 2013). In contrast, IB4+ and CGRP+ neurons relay nociception through small-diameter unmyelinated axons that innervate secondary neurons in the superficial dorsal horn. Therefore, proprio-/mechanoreceptive axons require far more robust long-distance regeneration than nociceptive axons for functional recovery. Moreover, myelinated proprio-/mechanoreceptive axons regenerate more poorly than nonmyelinated nociceptive axons (Tessler et al., 1988; Guseva and Chelyshev, 2006; Han et al., 2017). Therefore, AAV2-GFP provides a unique opportunity to study selectively regeneration of proprio-/mechanoreceptive axons whose regenerative capacity is particularly weak and needs robust augmentation.

Strategies for complete lesions and comprehensive evaluation of DR regeneration

Regeneration studies in animals suffer from conflicting and non-reproducible results, in part due to incomplete lesions which lead to mistakenly interpreting spared axons as regenerating axons (Steward et al., 2003; Steward et al., 2012). Completely crushing a DR is particularly demanding because DRs are tightly attached to spinal cord surfaces in flat, transparent layers (Han et al., 2012; Son, 2015). Various surgical methods have been applied to facilitate complete lesions, such as repetitive and bidirectional crushing of a root (Steinmetz et al., 2005; Wu et al., 2016). However, there have been no assays that would confirm that a surgery was successful.

We used two strategies to avoid spared axons. In one, we first crushed DRs and then micro-injected AAV2-GFP into DRGs (Figure 2A). This strategy transduces only axons proximal to the lesion, leading to labeling of regenerating, but not degenerating, distal stump axons. This is important because distal axons are very slowly removed in the CNS (Vargas and Barres, 2007), and thus can be mistakenly identified as regenerating axons in a conventional immunostaining

analysis of transverse sections. In the second strategy, after euthanizing a mouse typically at 2 weeks post injury (wpi), we harvested spinal cords with attached DRs and DRGs, examined them first in wholemounts and excluded those with poor viral infections. We then carefully examined the properly labeled wholemounts and confirmed that lesions were complete (e.g., Figure 2B). We excluded those containing spared axons with the following characteristics: present in groups of only a few, relatively straight and extremely lengthy axon trajectories that extend along the entire length of the spinal cord and terminate with no discernable axon endings (e.g., Figure 2C; Han et al., 2012). A highly experienced surgeon performed all the root crushes. Nevertheless, incomplete lesions occurred in ~20% of the animals, typically because axons had been spared in the outermost dorsal rootlets (Figure 2C).

The wholemounts also enabled us to examine an unprecedented number of regenerating proprio-/mechanoreceptive axons from multiple injured roots. After a complete root crush in a wildtype (WT) mouse, hundreds of GFP+ axons all terminated at similar locations along the length of the dorsolateral spinal cord (Figure 2B). Consistent with earlier studies of tissue sections (Golding et al., 1999; Di Maio et al., 2011), wholemounts revealed that GFP+ axons crossed the astrocyte:PNS border and terminated mostly within ~200µm of the border, forming a narrow front of axon tips (Figure 2D). Following wholemount assessment, we prepared serial transverse sections and evaluated regeneration of DR axons, across the DREZ and within the spinal cord. In WT mice, axons frequently grew dorsally along the growth-permissive pia matter (Figure 2E; arrowheads). We occasionally observed axons located subdurally several hundred microns past the astrocyte:PNS border (Figure 2E; arrow). Most axons, however, were located within ~100µm of the border and only a few axons reached ~200µm (Figure 2F). In the present comparative analyses, we considered axons that grew farther than 100 µm as having penetrated the DREZ. When astrocytes could not be co-immunostained, the border was approximated based on the greater abundance of cell nuclei in the PNS than CNS (Figure 2E).

Genetic deletion of Nogo, MAG and OMgp elicits no regeneration across the DREZ

We first investigated the effects of simultaneous deletion of myelin-associated inhibitors by examining global tKO mice lacking Nogo isoforms (A, B, C), MAG and OMgp. These mice were initially raised on a mixed background, extensively characterized and used to study spinal

cord regeneration (Lee et al., 2010). Our examination of these non-congenic tKO mutants revealed no enhanced regeneration of DR axons across the DREZ (data not shown). To overcome possible complications due to genetic background (Montagutelli, 2000; Tedeschi et al., 2017), we subsequently obtained Nogo/OMgp double KO and MAG KO mice raised on a C57BL/6 background and bred them to generate congenic Nogo/MAG/OMgp tKO mice, which we confirmed by tail genotyping (Figure 3A). Congenic tKO mice were viable and fertile, with no gross abnormalities. They were intercrossed to generate additional 2-3 month- old tKO mice; age matched C57BL/6 mice were used as controls.

To examine DR regeneration, we unilaterally crushed L4 and L5 DRs ~3-5 mm from the DREZ and then microinjected high-titer AAV2-GFP into the ipsilateral L4 and L5 DRGs (Figure 3B). In this crush injury model, proximal axons of large, NF+ neurons are capable of regenerating across the injury site and growing along the root at ~1.5 mm/day until they are rapidly immobilized at the DREZ, ~4 days post injury (Di Maio et al., 2011). We examined WT and tKO at 2 wpi, which provides axons sufficient time to penetrate the DREZ if they are competent to do so. Wholemount examination of Nogo/MAG/OMgp tKO mice revealed many brightly labeled axons that extended along the L4 and L5 roots (Figure 3C), as they did also in WT mice (Figure 2B). In both tKO and WT mice, however, most GFP+ axons terminated at similar longitudinal locations near the astrocyte:PNS border. Some axons extended substantially longer processes dorsally toward the spinal cord midline (Figure 3C; arrow). However, similar axons were also frequent in WT, and their incidence and length were not noticeably different in tKO and WT mice. We next examined serial transverse sections of L4 and L5 spinal cords prepared from tKO mice. No sections revealed GFP+ axons that crossed the DREZ and grew deep into the spinal cord. Most axons stopped at the DREZ, within ~100μm of the astrocytic border, as in WT (Figure 3D, 3E). Axons that extended longer distances grew along the growth-permissive pia matter (Figure 3D; arrowheads), as in WT (Figure 2E). Thus, genetic elimination of three major myelin inhibitors did not enable GFP+ axons to cross the DREZ. These results suggest that inhibiting myelin associated growth inhibitors is insufficient for proprio-/mechanoreceptive axons to penetrate the DREZ.

Supplementary CSPG removal enables minimal regeneration across the DREZ in tKO mice

The limited regeneration across the DREZ in Nogo/MAG/OMgp tKO could be due to redundant inhibition by CSPGs that by themselves are capable of arresting axons at the DREZ. Conversely, CSPG removal might induce only minimal regeneration (Steinmetz et al., 2005; Wu et al., 2016) due to redundant and potent inhibition by myelin inhibitors. To test this possibility, we attenuated CSPGs in Nogo/MAG/OMgp tKO using lentivirus encoding Chondroitinase ABC (LV-chABC). ChABC promotes axon regrowth by digesting growth-inhibitory glycosaminoglycan (GAG) chains on CSPGs (Muir et al., 2019). We unilaterally crushed L4 and L5 DRs of Nogo/MAG/OMgp tKO, microinjected AAV2-GFP into the L4 and L5 DRGs, and injected high-titer LV-ChABC into the ipsilateral dorsal horn at multiple locations rostrocaudally along the L4-L5 DREZ (Figure 4A). Two weeks after injury, wholemounts of ChABC-expressed tKO mice appeared similar to those of WT mice: most GFP+ axons terminated near the astrocytic border (Figure 4B). We used CS56 antibody immunostaining to confirm that LV-ChABC effectively removed the inhibitory sulfated GAG chains on CSPGs (Figure 4C). Consistent with previous observations (Han et al., 2017), CSPG degradation was restricted to the dorsal horn on the injected side of the spinal cord (Figure 4C; asterisks). Notably, CSPGs were rapidly and markedly upregulated in Schwann cells after DR crush, resulting in far brighter CS-56 immunoreactivity in the PNS than in the CNS (data not shown). We observed considerable CS-56 immunoreactivity associated with Schwann cells near the DREZ in ChABC-expressed tKO mice (Figure 4C'; arrowhead). However, the intensity of immunoreactivity was markedly reduced compared to that in non-treated tKO mice, further suggesting that CSPGs at the DREZ were markedly attenuated by LV-ChABC.

Most of the serial transverse sections of L4 and L5 DREZ also showed DR axons arrested at the DREZ and were virtually indistinguishable from those of WT mice. Some sections exhibited a few GFP+ axons located slightly deeper in the dorsal funiculus; such axons were not observed in WT or tKO (Figure 4C'; arrows). These axons were within 200μm of the astrocytic border and constituted only ~10% of GFP+ axons (Figure 4D), however, suggesting that additional attenuation of CSPGs in Nogo/MAG/OMgp tKO only modestly promoted regeneration across the DREZ.

Chronic regeneration failure at the DREZ despite absence of Nogo/MAG/OMgp and CSPGs

Concurrent ablation of myelin inhibitors and CSPGs only minimally enhanced regeneration, as assessed at 2 wpi, enabling only ~10% GFP+ axons to reach intraspinally ~100μm past the DREZ. Additional axons may continue to penetrate the DREZ and grow within the spinal cord lacking myelin inhibitors and CSPGs. To investigate this possibility and the chronic effects of targeting myelin inhibitors and CSPGs, we next examined WT, Nogo/MAG/OMgp tKO and ChABC-expressed tKO mice at 4 wpi (Figure 5A). Consistent with earlier studies that demonstrated rapid and persistent immobilization of DR axons at the DREZ (Golding et al., 1996; Di Maio et al., 2011), WT mice exhibited no enhanced regeneration across the DREZ at 4 wpi, as examined in wholemounts (Figure 5B) or in transverse sections (Figure 5C). There was, however, a statistically insignificant increase in DR axons at the DREZ (Figure 5D).

Similarly, in Nogo/MAG/OMgp tKO at 4 wpi (Figure 5E, 5F, 5G), we found no qualitative or quantitative evidence that two additional weeks after injury enabled more axons to penetrate the DREZ. This observation suggests that DR axons were chronically immobilized as they entered the DREZ despite the absence of myelin inhibitors.

Likewise, ChABC-expressed Nogo/MAG/OMgp tKO mice exhibited little or no enhanced regeneration at 4 wpi, as examined in wholemounts (Figure 5H) and transverse sections (Figure 5I). We observed no increase in GFP+ axons that crossed the DREZ, indicating that no additional axons penetrated the DREZ and that those axons intraspinally located at 2 wpi (~10% GFP+ axons) did not extend further within the spinal cord lacking CSPGs. We observed significantly more axons at the DREZ in ChABC-expressed Nogo/MAG/OMgp tKO mice at 4 wpi than at 2 wpi (Figure 5J) or than in WT or Nogo/MAG/OMgp tKO mice at 4 wpi (Figure 5K). Notably, however, these GFP+ axons remained at the DREZ, indicating that prolonged attenuation of CSPGs did not enable them to penetrate the DREZ lacking Nogo, MAG and OMgp.

We also examined regeneration of CGRP+ nociceptive axons, which are not discernably labeled by AAV2-GFP. As anticipated, it was often not possible, as noted in WT mice at 2 wpi, to evaluate intraspinal regeneration on sections due to punctate residual CGRP immunoreactivity associated with superficial laminae of the ipsilateral dorsal horn, particularly in Lissauer's tract (Figure 2E: asterisks). Dorsal funiculus above the dorsal horn, however, largely lacked CGRP+ immunoreactivity, indicating little if any penetration of CGRP+ axons through the DREZ at 2 wpi in WT mice (Figure 2E). Similarly, dorsal funiculus lacked CGRP immunoreactivity at 4 wpi in WT (Figure 5C), Nogo/MAG/OMgp tKO (Figure 5F) and ChABC-expressed Nogo/MAG/OMgp tKO mice (Figure 5I). CGRP immunoreactivity in superficial laminae of these mice at 4 wpi appeared similar to that in WT mice at 2 wpi. Moreover, it was not directly connected to CGRP+ axons at the DREZ on any sections, indicating that no axons reached superficial laminae directly through the DREZ. Thus, CGRP+ axons also stop at the DREZ even with concurrent prolonged absence of myelin inhibitors and CSPGs. Collectively, these results demonstrate that both myelinated and unmyelinated DR axons stop at the DREZ and continue to be immobilized, even if myelin inhibitors and CSPGs are simultaneously removed. Therefore, the minimal regeneration observed in earlier studies targeting CSPGs was not due to redundant inhibition by myelin associated inhibitors. Instead, these findings suggest that neither myelin inhibitors nor CSPGs are critical in preventing regeneration of DR axons at the DREZ.

DR axons fail to penetrate the DREZ in Nogo/MAG/OMgp tKO even after a conditioning lesion

Although genetic deletion of myelin inhibitors alone does not permit DR axons to grow through the DREZ, it may enable conditioned axons with enhanced growth capacity to do so. To test this possibility, we performed a nerve conditioning lesion by crushing the sciatic nerve 10 days before crushing the L4 and L5 roots (Figure 6A). At 2 wpi, wholemounts of GFP+ axons in conditioned Nogo/MAG/OMgp tKO mice did not show noticeably enhanced penetration of the DREZ (Figure 6B). Accordingly, serial transverse sections occasionally exhibited a few axons that reached dorsolateral grey matter (Figure 6C: arrows), but most GFP+ axons failed to penetrate the DREZ (Figure 6C, 6D). Dorsal funiculus lacked CGRP immunoreactivity, suggesting that conditioned CGRP+ axons also failed to penetrate the DREZ. Compared to WT and tKO mice, conditioned tKO mice exhibited significantly more axons at the DREZ,

presumably reflecting enhanced regeneration in the peripheral portion of the DR (Di Maio et al., 2011). We rarely observed axons extended more than >200μm from the astrocytic border in conditioned tKO mice, as in WT and non-conditioned tKO mice (Figure 6D). Therefore, removal of myelin associated inhibitors does not enable even conditioned axons to regenerate beyond the DREZ.

Supplementary CSPG removal does not enhance intraspinal penetration in conditioned tKO

We next asked whether additional attenuation of CSPGs in Nogo/MAG/OMgp tKO mice would enable robust penetration of conditioned axons through the DREZ. To test this possibility, we injected LV-ChABC rostrocaudally in dorsal horns along the L4-L5 DREZ in Nogo/MAG/OMgp tKO mice which received a nerve conditioning lesion 10 days before crushing L4 and L5 roots (Figure 7A). Surprisingly, at 2 wpi, despite the concurrent degradation of CSPGs, conditioned axons of Nogo/MAG/OMgp tKO mice largely remained near the astrocytic border in wholemounts (Figure 7B). CS-56 antibody immunostaining confirmed effective removal of CSPGs in dorsal horns (Figure 7C). Serial transverse sections occasionally revealed GFP+ axons that reached dorsolateral grey matter (Figure 7D; arrows), but most axons remained at the DREZ within ~100μm of the border (Figure 7E). Similarly, we observed no noticeably enhanced regeneration of CGRP+ axons in conditioned/ChABC-expressed Nogo/MAG/OMgp tKO (Figure 7D). These results demonstrate that additional removal of CSPGs did not enable significantly more GFP+ axons to penetrate the DREZ in conditioned tKO mice. In sum, CSPG degradation and/or a conditioning lesion increases the number of axons at the DREZ in Nogo/MAG/OMgp tKO mutants, but most of these axons fail to cross the DREZ (Figure 7F). CSPG removal improves penetration of conditioned or unconditioned axons in tKO mutant, but the effect is modest, enabling only ~10% axons to extend ~100μm past the DREZ (Figure 7F). These results collectively suggest that myelin inhibitors and CSPGs are not the primary factors that arrest even conditioned DR axons at the DREZ.

Nogo/MAG/OMgp removal enhances GDNF-induced intraspinal growth of DR axons

Our findings that even conditioned DR axons penetrate only modestly through the DREZ in ChABC-expressed tKO raise the possibility that myelin inhibitors and CSPGs are not

significantly inhibitory to DR axons. Alternatively, they may hinder regeneration within the spinal cord, although their inhibition is not sufficient to block axons at the DREZ. To test this possibility, we applied a treatment that enabled axons to penetrate the DREZ and then examined if their intraspinal regeneration was altered in Nogo/MAG/OMgp tKO mice with or without additional attenuation of CSPGs. Intraspinal expression of neurotrophic factors elevates regenerative capacity and chemotropically attracts DR axons, enabling them to cross the DREZ (Ramer et al., 2000; Iwakawa et al., 2001; Kelamangalath et al., 2015). When expressed virally within the spinal cord, GDNF promoted penetration of large-diameter DR axons through the DREZ and further into the spinal cord (Kelamangalath et al., 2015; Han et al., 2017).

We microinjected lentivirus expressing GDNF (LV-GDNF), extensively used in earlier studies (Deng et al., 2013; Zhang et al., 2013; Kelamangalath et al., 2015; Han et al., 2017), into the dorsal horn rostrocaudally along the L4-L5 DREZ at the time of DR crush in WT (Figure 8A) or Nogo/MAG/OMgp tKO mice (Figure 8E). At 2 wpi, wholemounts of GDNF-expressed WT mice did not show markedly enhanced regeneration into the spinal cord (Figure 8B). Serial sections, however, frequently revealed GFP+ axons that crossed the DREZ and extended further into the dorsal funiculus and grey matter (Figure 8C). Quantification indicated that ~50% of GFP+ axons penetrated the DREZ and extended up to ~300μm from the astrocytic border (Figure 8D). Consistent with an earlier study (Iwakawa et al., 2001), we also observed numerous CGRP+ axons in the dorsal funiculus, indicating regeneration of nociceptive axons across the DREZ.

Compared to GDNF-expressed WT mice, wholemounts of GDNF-expressed Nogo/MAG/OMgp tKO mice frequently revealed areas of the DREZ that exhibited conspicuously intense GFP fluorescence, likely due to densely accumulated subdural GFP+ axons (Figure 8F; arrows). Indeed, serial sections often displayed abundant GFP+ axons at the DREZ and within the spinal cord, indicating markedly enhanced intraspinal regeneration in tKO mutants (Figure 8G). We also observed bright CGRP+ immunoreactivity in deep dorsal laminae which are usually devoid of residual CGRP+ staining, presumably indicating enhanced regeneration of nociceptive axons (Figure 8G; asterisk). The extent of intraspinal regeneration markedly exceeded that observed in GDNF-expressed WT mice, nearly tripling the number of GFP+ axons counted at 200μm centrally from the border (Figure 8H). Notably, many more GFP+ axons were present at the

DREZ and within the spinal cord than peripherally along the root (Figure 8H). These results, together with the observation of GFP+ axons densely accumulated at the DREZ in wholemounts, suggest that genetic deletion of Nogo/MAG/OMgp may have enhanced intraspinal regeneration of DR axons largely by facilitating formation of additional axon branches (Figure 8H). Collectively, these findings indicate that myelin inhibitors are indeed inhibitory to DR axons and can substantially restrict their regeneration within the spinal cord. Importantly, however, genetic deletion of myelin inhibitors does not by itself induce intraspinal regeneration but promotes intraspinal regrowth of DR axons that has been elicited by a combinatory treatment.

CSPG removal further enhances GDNF-elicited intraspinal regeneration in tKO

Lastly, we investigated the synergistic effect of CSPG degradation on GDNF-elicited regeneration in Nogo/MAG/OMgp tKO mutants to determine if CSPGs also restrict regrowth of DR axons. We micro-injected LV-GDNF and LV-ChABC into dorsal horns and AAV2-GFP into DRGs at the time of L4/L5 root crush (Figure 9A). At 2 wpi, wholemounts of GDNF/ChABC-expressed tKO mice revealed broader areas of the DREZ and the CNS with intense GFP fluorescence than in GDNF-expressed tKO mice (Figure 9B; arrows). Moreover, many GFP+ axons extended rostrocaudally close to the midline (Figure 9B; arrowheads), further evidence of enhanced intraspinal penetration and regeneration. Accordingly, transverse sections frequently showed GFP+ axons densely filling a broader and deeper area of the dorsal horn (Figure 9C, 9D). CGRP immunoreactivity on some sections was conspicuously bright, dense and notably restricted to the superficial laminae, similar to CGRP immunoreactivity on the contralateral uninjured side (Figure 9D). Compared to GDNF-expressed tKO, GDNF/ChABC-expressed tKO mice showed significantly more GFP+ axons in deeper portions of the dorsal horn (Figure 9E). These results show that additional removal of CSPGs synergistically enhanced intraspinal regeneration elicited by GDNF in Nogo/MAG/OMgp tKO mice. Therefore, CSPGs, like myelin inhibitors, restricts intraspinal regrowth of DR axons although it does not constrain them at the DREZ.

DISCUSSION

Using novel multifaceted strategies, we compared DR regeneration in WT, Nogo/MAG/OMgp tKO, ChABC-expressed tKO, GDNF-expressed tKO and GDNF/ChABC-expressed tKO mice,

either with or without a conditioning lesion. Co-eliminating myelin inhibitors and CSPGs elicited only minimal intraspinal penetration, even after an additional conditioning lesion. Their absence, however, synergistically enhanced GDNF-elicited intraspinal axon growth. These findings suggest that a mechanism independent of myelin inhibitors and CSPGs vigorously blocks axons at the DREZ, and that this barrier can be overcome by elevating neuronal growth capacity above that achieved by a conditioning lesion. They also suggest that therapeutically targeting myelin inhibitors and CSPGs alone can enhance, but will not induce, intraspinal regeneration of primary sensory axons.

Various AAV vectors, including AAV2, demonstrate neuronal tropism (Mason et al., 2010; Fischer et al., 2011). Several AAV serotypes exhibit differential tropism for specific subpopulations of DRG neurons: AAV6 preferentially transduces small-sized neurons; AAV5, 8, and 9, large neurons (Jacques et al., 2012; Yu et al., 2013; Wu et al., 2016; Kubota et al., 2019). We found that AAV2 preferentially transduces NF+ neurons. Approximately 80% of GFP+ neurons were NF+, although only ~50% of lumbar DRG neurons are NF+ in mice (Li et al., 2016). IB4+ neurons constituted only ~5% of GFP+ neurons whilst CGRP+ neurons accounted for ~30%. Because ~30% of CGRP+ neurons also express NF200 (Li et al., 2016), our results are likely an overestimation of CGRP+ neurons projecting nociceptive axons. GFP expression in superficial dorsal laminae (I-IIi), where nociceptive afferents terminate, was almost undetectable (Figure 1E). It appears, therefore, that the predominant transduction of NF+ neurons and minimal expression of GFP in CGRP+ axons make AAV2-GFP a useful tracer of proprioceptive and mechanoreceptive axons.

Axon sparing has hampered consistent and conclusive studies with the widely used DR crush model (Smith et al., 2012). We found that complete crushing is difficult even in fluorescent mice whose axons are well visualized. Furthermore, improperly crushed axons often recover connectivity with distal axons (Di Maio et al., 2011; Han et al., 2012). Here we studied L4-L5 roots because in our experience DR crush is more likely to spare cervical than lumbar roots. In addition, we used wholemount preparations to detect spared axons, which is possible because AAV2-GFP brightly labels numerous axons. Importantly, however, wholemount assessment

417 does not guarantee complete lesions because viral transduction does not label all axons and
418 spared axons that are deeply located may be overlooked.
419
420 Wholemounts also permitted simultaneous assessment of many axons in multiple roots.
421 Markedly enhanced regeneration appeared as areas with unusually bright, dense GFP
422 fluorescence. Rostrally extending bundles of GFP+ axons were also observed when intraspinal
423 penetration exceeded 50%. These features require many intraspinally regenerating axons and
424 therefore provide convincing evidence of robustly enhanced intraspinal penetration.
425 Accordingly, wholemount assay is particularly useful for studies such as the present one, which
426 uses a relatively small number of animals. We excluded mice for various reasons, including
427 incomplete lesions and poor axon labeling, and used 3-8 mice per cohort to compare a total of 10
428 different animal groups. Nevertheless, no tKO, ChABC-expressed tKO, or conditioned/ChABC-
429 expressed tKO mice exhibited either fluorescent areas of densely populated axons or rostral axon
430 bundles. In contrast, these were consistent findings in all the wholemounts of GDNF-expressed
431 tKO and GDNF/ChABC-expressed tKO mice. Uniform absence or presence of these major
432 features in wholemounts is therefore useful to determine if a specific factor serves as a major
433 inhibitor or promoter of DR regeneration across the DREZ.
434
435 Wholemounts showed no such features and transverse sections revealed minimal intraspinal
436 penetration up to 4 wpi in Nogo/MAG/OMgp tKO with or without additional CSPG degradation.
437 More surprisingly, there was little enhancement even with conditioning lesions of ChABC-
438 expressed Nogo/MAG/OMgp tKO mice. Minimal enhancement was unlikely due to insufficient
439 removal of Nogo/MAG/OMgp or CSPGs. Most notably, GDNF robustly enhanced regeneration
440 in Nogo/MAG/OMgp tKO and produced even more regeneration in ChABC-expressed tKO
441 mice. These observations, together with earlier studies that demonstrated efficacy of the
442 Nogo/MAG/OMgp tKO and LV-ChABC (Curinga et al., 2007; Lee et al., 2010; Jin et al., 2011;
443 Han et al., 2017), indicate that penetration was not limited because of insufficient elimination of
444 Nogo, MAG, OMgp, CSPGs and/or undigested CSPG carbohydrate stubs (Lemons et al., 2003).
445 Our findings are consistent with earlier observations that degrading CSPGs alone (Steinmetz et
446 al., 2005; Wu et al., 2016), or in combination with conditioning lesions (Quaglia et al., 2008)
447 elicits minimal intraspinal penetration. Importantly, they demonstrate for the first time that the

minimal penetration elicited by the absence of CSPGs was unlikely due to synergistic restraint by myelin inhibitors.

Co-eliminating myelin inhibitors and CSPGs was insufficient to achieve DR regeneration into the spinal cord, even when combined with a conditioning lesion. These results contrast with the robust, long-distance functional regeneration of myelinated DR axons reported in earlier studies that targeted Nogo receptor or CSPG/CSPG receptors, with or without a conditioning lesion (Harvey et al., 2009; Peng et al., 2010; Cheah et al., 2016; Yao et al., 2019). Blocking inhibitors in adulthood may be more effective than eliminating them during development due to compensatory upregulation of other inhibitors (El-Brolosy and Stainier, 2017). It is noteworthy, however, that we removed CSPGs in adult tKO mice. Another possible explanation for the discrepancy is a species difference between mice and rats (Lee and Lee, 2013), but results have also conflicted in the same species. Additional myelin-associated inhibitors and ligands of Nogo and CSPG receptors have been identified (Zhang et al., 2009b; Dickendesher et al., 2012; Thiede-Stan and Schwab, 2015; Ohtake et al., 2018). However, CSPGs are the major additional ligands that bind to the Nogo receptor (Dickendesher et al., 2012), yet co-eliminating CSPGs and myelin inhibitors elicited little penetration. An alternative explanation is that these studies included incomplete lesions of varying extent, which were followed by acute or gradual functional recovery that did not require actual regeneration or relied on sprouting of spared axon terminals (Cafferty et al., 2008). We failed to find convincing evidence, in these reports, of axons penetrating the DREZ and regenerating for long distances, which would be necessary to support either course of functional regeneration.

Targeting Nogo, CSPGs or their receptors in rodent models of spinal cord injury promotes little regeneration of myelinated axons, such as corticospinal tract (Fink et al., 2015; Lang et al., 2015; Ito et al., 2018). However, their removal can significantly enhance the growth promotion of a combinatory treatment (Wang et al., 2012; DePaul et al., 2017; Wu et al., 2017). Consistent with these observations, we found that although eliminating myelin inhibitors alone did not induce intraspinal penetration, it markedly enhanced GDNF-elicited intraspinal axon growth. This intraspinal growth was further enhanced by concomitant removal of CSPGs, suggesting that both myelin inhibitors and CSPGs synergistically inhibit regrowth of DR axons within the spinal cord.

Notably, we also observed a significantly increased number of axons at the DREZ in GDNF-expressed tKO and in ChABC-expressed tKO mice. We infer, therefore, that myelin inhibitors and CSPGs also constrain regeneration at the DREZ, but their absence is insufficient to enable axons to cross the DREZ.

Myelin inhibitors and CSPGs are thought to stop axons at the DREZ by collapsing or trapping growth cones and inducing dystrophic endings (Li et al., 1996; Golding et al., 1999; Ramer et al., 2001; Tom et al., 2004; Smith et al., 2012). Our results revise this long-held view by suggesting the presence of inhibitory mechanism(s) of greater potency that arrest even conditioned axons and act independently of myelin inhibitors and CSPGs. One such inhibitory mechanism may be the expression of additional repellent cues that are upregulated at the axotomized DREZ (Andrews et al., 2009; Lindholm et al., 2017). Another possibility, which we favor, is that most axons are stabilized at the DREZ by forming aberrant synapses rather than dystrophic endings (Carlstedt, 1985; Liuzzi and Lasek, 1987; Stensaas et al., 1987; Di Maio et al., 2011; Son, 2015). We could not confirm this possibility in the present study because of the experimental challenges of differentiating dystrophic from synaptic endings, and in blocking aberrant synapse formation. However, we have obtained additional evidence for a synapse-based inhibitory mechanism that supports this notion (Kim et al., in preparation). Other possible, although less likely, mechanisms include lack of a growth-permissive/promoting substrate (Li et al., 2004; Han et al., 2017; Collins et al., 2019) and/or inadequate intrinsic growth ability of DRG neurons (Steinmetz et al., 2005; Nichols and Smith, 2020).

Conditioning lesioned DRG neurons have been extensively used for epigenetic, transcriptomic and proteomic studies of peripheral and central regeneration (Blesch et al., 2012; Li et al., 2015; Palmisano et al., 2019). We found that GDNF, but not a conditioning lesion, enabled intraspinal penetration in ChABC-expressed tKO mice. Therefore, a conditioning lesion does not sufficiently elevate regenerative capacity to overcome the potent myelin/CSPG-independent inhibitory mechanism(s). Although our results highlight the importance of sufficiently elevating regenerative potential, GDNF enhanced penetration of less than 50% DR axons. Moreover, the intraspinal regeneration it elicited in the absence of myelin inhibitors and CSPGs was apparently enhanced but did not appear sufficiently robust to power the long-distance regeneration required

for proprio-/mechanoreceptive axons. The DR regeneration induced by several other neurotrophic factors, cytokines and downstream effectors has been generally weaker than that elicited by GDNF in ChABC-expressed tKO mice (O'Donovan et al., 2014; Liu et al., 2016; Wu et al., 2016). Learning how to maximize the regenerative potential must be as important as understanding the myelin/CSPG-independent mechanism that powerfully halts axons at the DREZ, and perhaps also within the damaged spinal cord.

MATERIALS AND METHODS

Reagent type (species) or resource	Designation	Source or Reference	Identifiers	Additional Information
Strain, strain background (*Mus musculus*)	Nogo/OMgp double knockout	Dr. Binhai Zheng (UCSD)		Lee et al., 2010
Strain, strain background (*Mus musculus*)	MAG knockout	Dr. Jae K. Lee (U.Miami)	Stock #: 006865; RRID:IMSR JAX:006865	
Strain, strain background (*Mus*	C57BL/6J	The Jackson Laboratory	Stock #: 000664; RRID:IMSR JAX:000664	

musculus)				
Reagent	Vectashield	Vector Laboratories, Burlingame	H-100 RRID:AB2336789	
Viral reagent	scAAV2-eGFP	Dr. George M. Smith (Temple University)		Liu et al., 2014
Viral reagent	LV-chABC	Dr. George M. Smith (Temple University)		Curinga et al., 2007
Viral reagent	LV-GDNF	Dr. George M. Smith (Temple University)		Zhang et al., 2013
Antibody	anti-NF200 (rabbit polyclonal)	Sigma	#N4142 RRID:AB477272	IHC 1:500
Antibody	anti-IBA-biotin conjugate	Sigma	#L2140 RRID:AB2313663	IHC 1:200
Antibody	anti-CGRP (rabbit polyclonal)	Peninsula Labs	#T4032 RRID:AB2307330	IHC 1:2,000
Antibody	anti-GFP monoclonal	Avés Labs Inc.	#GFP-1020 RRID:AB10000240	IHC 1:500

Antibody	anti-GFAP (rabbit polyclonal)	Agilent	#N1506 RRID:AB10013482	IHC 1:500
Antibody	Alexa Fluor 647-goat anti-rabbit IgG secondary antibody	Invitrogen	#31573 RRID:AB2536183	IHC 1:400
Antibody	Fluorescein (FITC)-conjugated goat anti-rabbit IgG secondary antibody	Millipore	#AP307F RRID:AB92652	IHC 1:400
Antibody	Alexa Fluor 568-conjugated goat anti-mouse IgG_1 secondary antibody	Invitrogen	# A21124 RRID:AB141611	IHC 1:400
Antibody	rhodamine (TRITC) streptavidin secondary antibody	Jackson ImmunoResearch Labs Inc.	#016-020-084 RRID:AB2337237	IHC 1:400
Antibody	Alexa-Fluor 568-conjugated goat anti-rabbit	Invitrogen	#A11011 RRID:AB143157	IHC 1:400

	secondary antibody			
Antibody	Alexa Fluor 488-donkey anti-chicken IgG secondary antibody	Jackson ImmunoResearch Labs Inc.	#703-545-155 RRID:AB2340375	IHC 1:400
other	DAPI stain	Thermo Fisher Scientific	#D1306 RRID:AB2629482	IHC 1:1,000
Reagent	Nissl substance stain	Thermo Fisher Scientific	#N21482 RRID:AB2620170	IHC 1:200
software, algorithm	MetaMorph Image Analysis Software	Molecular Devices	RRID:SCR002368	
software, algorithm	AxioVision Imaging System	Zeiss	RRID:SCR002677	
software, algorithm	Axio Imager	Zeiss		
other	SP8 confocal microscope	Leica Microsystems	RRID:SCR018169	
software, algorithm	Imaris	Bitplane	RRID:SCR007370	
software, algorithm	Adobe Photoshop	Adobe Inc.	RRID:SCR014199	

software, algorithm	PRISM 8.0	GraphPad	RRID:SCR002798	

519

520 *Mice.* All animal care and procedures were conducted in accordance with the National Research
521 Council's Guide for the Care and Use of Laboratory Animals and approved by the Institutional
522 Animal Care and Use Committee at Lewis Katz School of Medicine at Temple University,
523 Philadelphia, PA, USA. Congenic Nogo/OMgp/MAG triple knockout mice were generated by
524 breeding congenic lines of Nogo/OMgp double knockout mice obtained from Dr. Binhai Zheng
525 (University of California at San Diego) and of MAG single knockout mice obtained from Dr. Jae
526 K. Lee (University of Miami). Male and female, 2-3 months old Nogo$^{-/-}$/OMgp$^{-/-}$/MAG$^{-/-}$ mice
527 and age-matched C57BL/6J mice (The Jackson Laboratory) were used. Mice were genotyped at
528 the time of weaning by tail clipping and PCR analysis using the primers described in earlier
529 studies (Li et al., 1994; Lee et al., 2010).

530

531 *Dorsal root crush.* Mice were anesthetized with an intraperitoneal injection of xylazine (8
532 mg/kg) and ketamine (120 mg/kg). Supplements were given during the procedure as needed.
533 Following a 2- to 3-cm-long incision in the skin of the back, the spinal musculature was reflected
534 and the L3–S1 spinal cord segments exposed by hemilaminectomies to prepare for unilateral L4–
535 L5 root crush. The cavity made by the laminectomies was perfused with warm sterile Ringer's
536 solution. A small incision was made in the dura overlying the L4 and L5 DR. A fine forceps
537 (Dumont #5; Fine Science Tools, Foster City, CA) was introduced subdurally and the DR
538 crushed for 10 s. To avoid scar formation and possible compression, we applied a piece of thin
539 SILASTIC membrane (Biobrane, Bertek Pharmaceuticals, Sugarland, TX) over the laminectomy
540 site and covered it with a layer of thicker artificial dura (Gore Preclude MVP Dura Substitute,
541 W.L. Gore and Associates, Flagstaff, AZ). The overlying musculature was closed with 5-0
542 sutures, and the skin closed with wound clips. All animals received subcutaneous injections of
543 saline (0.9% w/v NaCl) and buprenorphine (0.05 mg/kg) for postoperative pain management and
544 remained on a heating pad until fully recovered from anesthesia. Mice were perfused 2 or 4
545 weeks after the crush, and axon regeneration was analyzed in cryostat sections or in thin dorsal
546 slice preparations of whole spinal cord.

547

548 *Conditioning lesion by sciatic nerve crush.* DRG neurons were preconditioned by crushing the
549 sciatic nerve in the lateral thigh of the ipsilateral hind leg 10 days before the DRs were crushed.
550 Animals were anesthetized as described above; the skin and superficial muscle layer of the
551 midthigh were opened; and the sciatic nerve was crushed for 10 s with fine forceps (Dumont #5;
552 Fine Science Tools, Foster City, CA). The muscle and skin were then closed in layers and the
553 animals allowed to recover on a heating pad until fully awake.
554
555 *Production and microinjection of AAV2-GFP, LV-chABC and LV-GDNF.* Recombinant self-
556 complementary adeno-associated virus 2 (scAAV2) carrying eGFP was generated by helper
557 virus-free system (Ayuso et al., 2010) as described previously (Liu et al., 2014). Replication
558 deficient lentiviruses encoding either chABC (LV-chABC) or GDNF (LV-GDNF) used a pBOB
559 lentiviral expression vector with CMV-enhanced chicken β-actin (CAG) promoter. The
560 procedures to generate the viruses and their efficacy were described before: LV-chABC (Curinga
561 et al., 2007; Jin et al., 2011; Han et al., 2017); LV-GDNF (Zhang et al., 2009a; Deng et al., 2013;
562 Zhang et al., 2013; Kelamangalath et al., 2015; Han et al., 2017). AAV2-GFP was microinjected
563 into lumbar DRGs using a micropipette pulled to a diameter of 0.05 mm and a nanoinjector
564 (World Precision Instruments, Sarasota, FL). The viruses were injected at the time of DR crush.
565 For each injection, the micropipette was introduced 0.5 mm into the DRG and a total volume of
566 AAV (0.8 µl) containing >$2x10^{12}$ GC/ml injected over a 10 min period. The glass needle was left
567 in place for 2 min after each injection. For LV-GDNF, five injections of 0.3µl lentivirus (a total
568 of 2×10^{7} viral particles) were equally spaced rostrocaudally along the L4–L5 DREZ. Injections
569 were made at a rate of 100 nl/min at a depth of 0.25mm from the spinal cord dorsal surface.
570
571 *Tissue processing, selection and immunohistochemistry*. Two or four weeks after DR crush, mice
572 were sacrificed by an overdose of Euthasol and perfused transcardially with 0.9% saline
573 followed by 4% paraformaldehyde (PFA) in 0.1M phosphate buffer (PBS, pH=7.4). The spinal
574 cords with attached dorsal roots and DRGs were removed and examined in wholemounts to
575 exclude those tissues with poor transduction of AAV2-GFP and/or spared axons. Properly
576 lesioned and GFP+ tissues were first examined in wholemounts to assess DR regeneration across
577 the DREZ. Tissues were then processed for analysis on cryostat sections. One or two
578 representative tissues were processed for immunohistochemistry in spinal cord wholemounts.

For analysis on cryostat sections, spinal cords were post-fixed in 4% PFA overnight at 4°C and cryoprotected in 30% sucrose for 1-2 days. The tissues were then embedded in M-1 Embedding Matrix (Thermo Fisher Scientific, Waltham, MA), transversely sectioned at 20 µm using a cryostat (Leica Microsystems, Germany), and mounted directly on slides (Superfrost Plus, Fisher Scientific, Pittsburgh, PA). For immunolabeling, sections were rinsed three times in PBS for 30 min followed by 10 min incubation with 0.1 M glycine in PBS, and 15 min incubation with 0.2% Triton X-100, 2% bovine serum albumin (BSA) in PBS (TBP). Sections were incubated with primary antibodies overnight at 4°C, washed three times for 30 min with 2% BSA in PBS and incubated with secondary antibodies for 1 h at room temperature. After three rinses with PBS, sections were mounted in Vectashield (Vector Laboratories, Burlingame, CA) and stored at -20°C until examination. For wholemount immunostaining of spinal cords, spinal cords with attached DRs were post-fixed in 4% PFA for 2 h at 4°C and the dura mater removed. The spinal cord was then rinsed three times with PBS for 30 min, incubated for 10 min in 0.1M glycine in 2% BSA/PBS, and permeabilized with pre-cooled methanol at -20°C for 10 min. After extensive rinsing in PBS, the spinal cord was incubated with primary antibody diluted in TBP at room temperature overnight, rinsed thoroughly in TBP the following day, and incubated with secondary antibodies for 2 h at room temperature. After rinsing in PBS, a thin slice of dorsal spinal cord (~2 mm thick) with attached DR stumps was cut with a microscissors and mounted on slides in Vectashield (Vector Laboratories, Burlingame, CA).

Antibodies. Primary antibodies were used at the following concentrations for immunohistochemistry: rabbit anti-NF200 (1:500, Sigma, St. Louis, MO, #N4142), IB4-biotin conjugate (1:200, Sigma, St. Louis, MO, #L2140), rabbit anti-CGRP (1:2,000, Peninsula Labs, San Carlos, CA, #T4032), chicken anti-GFP (1:1,000, Avés Labs Inc., Davis, CA, #GFP-1020), rabbit anti-GFAP (1:500, Agilent, Santa Clara, CA, #N1506). Secondary antibodies used were Alexa Fluor 647-goat anti-rabbit IgG (1:400, Invitrogen, , Indianapolis, IN, #31573), Fluorescein (FITC)-conjugated goat anti-rabbit IgG (1:400, Millipore, Temecula, CA, AP307F), Alexa Fluor 568-conjugated goat anti-mouse IgG1 (1:400, Invitrogen, Indianapolis, IN, A21124), Alexa-Fluor 568-conjugated goat anti-rabbit (1:400, Invitrogen, Indianapolis, IN, #A11011), rhodamine (TRITC) streptavidin (1:400, Jackson ImmunoResearch Labs Inc., West Grove, PA, #016-020-084), or Alexa Fluor 488-donkey anti-chicken IgG (1:400, Jackson ImmunoResearch Labs Inc.,

West Grove, PA, #703-545-155). DAPI nucleic acid stain (1:1000, Thermo Fisher Scientific, Pittsburgh, PA, #D1306) for cell nuclei or Nissl substance stain (1:200, Thermo Fisher Scientific, Pittsburgh, PA, #N21482) for neuronal cells was used to counterstain prior to final wash steps in PBS.

Microscopy and image acquisition. An Olympus BX53 microscope equipped with Orca-R2 CCD camera (Hamamatsu, Japan) controlled by MetaMorph Image Analysis Software (Molecular Devices, San Jose, CA) was used to examine serial cryostat sections and dorsal wholemounts. Z stacked images were acquired using the Axio Imager (Zeiss, Germany) upright fluorescence microscope and AxioVision Imaging System (Zeiss, Germany) software or a SP8 confocal microscope (Leica Microsystems, Buffalo Grove, IL). All images were processed using Imaris (Bitplane, Windsor, CT) and Adobe Photoshop (Adobe Inc. San Jose, CA).

Analysis of regeneration across the DREZ. The location of the DREZ, the transitional zone between the CNS and PNS, was demarcated by GFAP immunostaining of astrocytes. The white dotted lines (e.g., Figure 1D, 1E) approximate the location of the outer (peripheral) border of the DREZ, as defined by GFAP immunolabeling of astrocytic processes that extend peripherally (termed here 'astrocyte:PNS border' or 'astrocytic border'). When GFAP was not immunolabeled, the astrocytic border was approximated based on the greater abundance of cell nuclei in the PNS than CNS. For comparative evaluation of regeneration across the DREZ, we considered that DR axons penetrated into the CNS when they extended at least 100μm beyond the astrocyte:PNS border. For quantitative analysis, digital images were captured from 3-6 representative, non-adjacent sections taken from L4 and L5 segments of each mouse (n=3-8 mice per cohort). A raw image was converted to a binary image using ImageJ with a threshold that appropriately separated GFP and background fluorescence. Lines were drawn at 100 μm before the border (in PNS territory), at the DREZ outer border, and at 100 μm intervals into CNS territory. The number of intersections of GFP+ axons at these distances was counted. The number of axons that crossed the outer border was normalized by the number of GFP+ axons counted at 100 μm before the border in the PNS, and then averaged by the number of evaluated sections and animals. This quantification resulted in the 'axon number index' that indicated the relative number and distance of axons that regenerated into the CNS in each group of mice.

Statistical analysis. All statistical analyses were performed using PRISM 8.0 (GraphPad, San Diego, CA.). Statistical analysis was by two-way repeated measures analysis of variance (ANOVA) with Tukey's multiple comparison tests. All data are presented as mean ± SD. Results were considered statistically significant if the p-value was < 0.05.

COMPETING INTERESTS

The authors declare no competing financial interests.

ACKNOWLEDGMENTS

We thank Drs. Alan Tessler, Matt Grove and Harun Noristiani for critical reading of the manuscript. We greatly thank Dr. Binhai Zheng for Nogo/MAG/OMgp triple and Nogo/OMgp double knockout mice, Dr. Jae Lee for MAG mutant mice, and Yingpeng Liu for technical assistance with LV-chABC and LV-GDNF.

FUNDINGS

This work was supported by NIH NINDS (NS079631) and Shriners Hospitals for Children (86600, 84050) to Y.-J.S.

REFERENCES

Andrews, M. R., Czvitkovich, S., Dassie, E., Vogelaar, C. F., Faissner, A., Blits, B., Gage, F. H., ffrench-Constant, C., and Fawcett, J. W. (2009). Alpha9 integrin promotes neurite outgrowth on tenascin-C and enhances sensory axon regeneration. *J Neurosci, 29*(17), 5546-5557. doi:29/17/5546 [pii] 10.1523/JNEUROSCI.0759-09.2009

Ayuso, E., Mingozzi, F., and Bosch, F. (2010). Production, purification and characterization of adeno-associated vectors. *Curr Gene Ther, 10*(6), 423-436.

Blesch, A., Lu, P., Tsukada, S., Alto, L. T., Roet, K., Coppola, G., Geschwind, D., and Tuszynski, M. H. (2012). Conditioning lesions before or after spinal cord injury recruit

671 broad genetic mechanisms that sustain axonal regeneration: superiority to camp-mediated
672 effects. *Exp Neurol, 235*(1), 162-173. doi:10.1016/j.expneurol.2011.12.037

673 Cafferty, W. B., Bradbury, E. J., Lidierth, M., Jones, M., Duffy, P. J., Pezet, S., and McMahon,
674 S. B. (2008). Chondroitinase ABC-mediated plasticity of spinal sensory function. *J*
675 *Neurosci, 28*(46), 11998-12009. doi:10.1523/jneurosci.3877-08.2008

676 Cafferty, W. B., Yang, S. H., Duffy, P. J., Li, S., and Strittmatter, S. M. (2007). Functional
677 axonal regeneration through astrocytic scar genetically modified to digest chondroitin
678 sulfate proteoglycans. *J Neurosci, 27*(9), 2176-2185. doi:10.1523/jneurosci.5176-06.2007

679 Carlstedt, T. (1985). Regenerating axons form nerve terminals at astrocytes. *Brain Res, 347*(1),
680 188-191. doi:0006-8993(85)90911-4 [pii]

681 Carlstedt, T. (2008). Root repair review: basic science background and clinical outcome. *Restor*
682 *Neurol Neurosci, 26*(2-3), 225-241.

683 Cheah, M., Andrews, M. R., Chew, D. J., Moloney, E. B., Verhaagen, J., Fässler, R., and
684 Fawcett, J. W. (2016). Expression of an Activated Integrin Promotes Long-Distance
685 Sensory Axon Regeneration in the Spinal Cord. *J Neurosci, 36*(27), 7283-7297.
686 doi:10.1523/jneurosci.0901-16.2016

687 Chong, M. S., Woolf, C. J., Haque, N. S. K., and Anderson, P. N. (1999). Axonal regeneration
688 from injured dorsal roots into the spinal cord of adult rats. *Journal of Comparative*
689 *Neurology, 410*(1), 42-54.

690 Collins, A., Ibrahim, A., Li, D., Liadi, M., and Li, Y. (2019). Reconstruction of the Damaged
691 Dorsal Root Entry Zone by Transplantation of Olfactory Ensheathing Cells. *Cell*
692 *Transplant, 28*(9-10), 1212-1219. doi:10.1177/0963689719855938

693 Curinga, G. M., Snow, D. M., Mashburn, C., Kohler, K., Thobaben, R., Caggiano, A. O., and
694 Smith, G. M. (2007). Mammalian-produced chondroitinase AC mitigates axon inhibition
695 by chondroitin sulfate proteoglycans. *J Neurochem, 102*(1), 275-288. doi:JNC4530
696 [pii]10.1111/j.1471-4159.2007.04530.x

Deng, L. X., Deng, P., Ruan, Y., Xu, Z. C., Liu, N. K., Wen, X., Smith, G. M., and Xu, X. M. (2013). A novel growth-promoting pathway formed by GDNF-overexpressing Schwann cells promotes propriospinal axonal regeneration, synapse formation, and partial recovery of function after spinal cord injury. *J Neurosci, 33*(13), 5655-5667. doi:10.1523/jneurosci.2973-12.2013

DePaul, M. A., Lin, C. Y., Silver, J., and Lee, Y. S. (2017). Combinatory repair strategy to promote axon regeneration and functional recovery after chronic spinal cord injury. *Sci Rep, 7*(1), 9018. doi:10.1038/s41598-017-09432-6

Di Maio, A., Skuba, A., Himes, B. T., Bhagat, S. L., Hyun, J. K., Tessler, A., Bishop, D., and Son, Y. J. (2011). In Vivo Imaging of Dorsal Root Regeneration: Rapid Immobilization and Presynaptic Differentiation at the CNS/PNS Border. *J Neurosci, 31*(12), 4569-4582. doi:31/12/4569 [pii]

10.1523/JNEUROSCI.4638-10.2011

Dickendesher, T. L., Baldwin, K. T., Mironova, Y. A., Koriyama, Y., Raiker, S. J., Askew, K. L., Wood, A., Geoffroy, C. G., Zheng, B., Liepmann, C. D., Katagiri, Y., Benowitz, L. I., Geller, H. M., and Giger, R. J. (2012). NgR1 and NgR3 are receptors for chondroitin sulfate proteoglycans. *Nat Neurosci, 15*(5), 703-712. doi:10.1038/nn.3070

El-Brolosy, M. A., and Stainier, D. Y. R. (2017). Genetic compensation: A phenomenon in search of mechanisms. *PLoS Genet, 13*(7), e1006780. doi:10.1371/journal.pgen.1006780

Fink, K. L., Strittmatter, S. M., and Cafferty, W. B. (2015). Comprehensive Corticospinal Labeling with mu-crystallin Transgene Reveals Axon Regeneration after Spinal Cord Trauma in ngr1-/- Mice. *J Neurosci, 35*(46), 15403-15418. doi:10.1523/jneurosci.3165-15.2015

Fischer, G., Kostic, S., Nakai, H., Park, F., Sapunar, D., Yu, H., and Hogan, Q. (2011). Direct injection into the dorsal root ganglion: technical, behavioral, and histological observations. *J Neurosci Methods, 199*(1), 43-55. doi:10.1016/j.jneumeth.2011.04.021

723 Golding, J. P., Bird, C., McMahon, S., and Cohen, J. (1999). Behaviour of DRG sensory neurites
724 at the intact and injured adult rat dorsal root entry zone: postnatal neurites become
725 paralysed, whilst injury improves the growth of embryonic neurites. *Glia, 26*(4), 309-323.
726 doi:10.1002/(SICI)1098-1136(199906)26:4<309::AID-GLIA5>3.0.CO;2-0 [pii]

727 Golding, J. P., Shewan, D., Berry, M., and Cohen, J. (1996). An in vitro model of the rat dorsal
728 root entry zone reveals developmental changes in the extent of sensory axon growth into
729 the spinal cord. *Molecular and Cellular Neuroscience, 7*(3), 191-203.
730 doi:10.1006/mcne.1996.0015

731 Griffin, J. M., and Bradke, F. (2020). Therapeutic repair for spinal cord injury: combinatory
732 approaches to address a multifaceted problem. *EMBO Mol Med, 12*(3), e11505.
733 doi:10.15252/emmm.201911505

734 Guo, W. L., Qu, W. R., Zeng, L. N., Qi, Z. P., Huang, C., Zhu, Z., and Li, R. (2019). l-Theanine
735 and NEP1-40 promote nerve regeneration and functional recovery after brachial plexus
736 root avulsion. *Biochem Biophys Res Commun, 508*(4), 1126-1132.
737 doi:10.1016/j.bbrc.2018.11.124

738 Guseva, D., and Chelyshev, Y. (2006). The Plasticity of the DRG Neurons Belonging to
739 Different Subpopulations After Dorsal Rhizotomy. *Cell Mol Neurobiol, 26*(7-8), 1223-
740 1232.

741 Han, S. B., Kim, H., Lee, H., Grove, M., Smith, G. M., and Son, Y. J. (2017). Postinjury
742 Induction of Activated ErbB2 Selectively Hyperactivates Denervated Schwann Cells and
743 Promotes Robust Dorsal Root Axon Regeneration. *J Neurosci, 37*(45), 10955-10970.
744 doi:10.1523/JNEUROSCI.0903-17.2017

745 Han, S. B., Kim, H., Skuba, A., Tessler, A., Ferguson, T., and Son, Y. J. (2012). Sensory Axon
746 Regeneration: A Review from an in vivo Imaging Perspective. *Exp Neurobiol, 21*(3), 83-
747 93. doi:10.5607/en.2012.21.3.83

748 Harvey, P. A., Lee, D. H., Qian, F., Weinreb, P. H., and Frank, E. (2009). Blockade of Nogo
749 receptor ligands promotes functional regeneration of sensory axons after dorsal root
750 crush. *J Neurosci, 29*(19), 6285-6295. doi:10.1523/jneurosci.5885-08.2009

751 Ito, S., Nagoshi, N., Tsuji, O., Shibata, S., Shinozaki, M., Kawabata, S., Kojima, K., Yasutake,
752 K., Hirokawa, T., Matsumoto, M., Takei, K., Nakamura, M., and Okano, H. (2018).
753 LOTUS Inhibits Neuronal Apoptosis and Promotes Tract Regeneration in Contusive
754 Spinal Cord Injury Model Mice. *eNeuro, 5*(5). doi:10.1523/eneuro.0303-18.2018

755 Iwakawa, M., Mizoi, K., Tessler, A., and Itoh, Y. (2001). Intraspinal implants of fibrin glue
756 containing glial cell line-derived neurotrophic factor promote dorsal root regeneration
757 into spinal cord. *Neurorehabil Neural Repair, 15*(3), 173-182.
758 doi:10.1177/154596830101500304

759 Jacques, S. J., Ahmed, Z., Forbes, A., Douglas, M. R., Vigenswara, V., Berry, M., and Logan, A.
760 (2012). AAV8(gfp) preferentially targets large diameter dorsal root ganglion neurones
761 after both intra-dorsal root ganglion and intrathecal injection. *Mol Cell Neurosci, 49*(4),
762 464-474. doi:10.1016/j.mcn.2012.03.002

763 Jin, Y., Ketschek, A., Jiang, Z., Smith, G., and Fischer, I. (2011). Chondroitinase activity can be
764 transduced by a lentiviral vector in vitro and in vivo. *J Neurosci Methods, 199*(2), 208-
765 213. doi:10.1016/j.jneumeth.2011.05.007

766 Kaiser, R., Waldauf, P., Ullas, G., and Krajcová, A. (2020). Epidemiology, etiology, and types of
767 severe adult brachial plexus injuries requiring surgical repair: systematic review and
768 meta-analysis. *Neurosurg Rev, 43*(2), 443-452. doi:10.1007/s10143-018-1009-2

769 Kelamangalath, L., Tang, X., Bezik, K., Sterling, N., Son, Y. J., and Smith, G. M. (2015).
770 Neurotrophin selectivity in organizing topographic regeneration of nociceptive afferents.
771 *Exp Neurol, 271*, 262-278. doi:10.1016/j.expneurol.2015.06.007

772 Kubota, S., Sidikejiang, W., Kudo, M., Inoue, K. I., Umeda, T., Takada, M., and Seki, K. (2019).
773 Optogenetic recruitment of spinal reflex pathways from large-diameter primary afferents

in non-transgenic rats transduced with AAV9/Channelrhodopsin 2. *J Physiol, 597*(19), 5025-5040. doi:10.1113/jp278292

Kwon, M. J., Shin, H. Y., Cui, Y., Kim, H., Thi, A. H., Choi, J. Y., Kim, E. Y., Hwang, D. H., and Kim, B. G. (2015). CCL2 Mediates Neuron-Macrophage Interactions to Drive Proregenerative Macrophage Activation Following Preconditioning Injury. *J Neurosci, 35*(48), 15934-15947. doi:10.1523/jneurosci.1924-15.2015

Lang, B. T., Cregg, J. M., DePaul, M. A., Tran, A. P., Xu, K., Dyck, S. M., Madalena, K. M., Brown, B. P., Weng, Y. L., Li, S., Karimi-Abdolrezaee, S., Busch, S. A., Shen, Y., and Silver, J. (2015). Modulation of the proteoglycan receptor PTPσ promotes recovery after spinal cord injury. *Nature, 518*(7539), 404-408. doi:10.1038/nature13974

Lee, D. H., and Lee, J. K. (2013). Animal models of axon regeneration after spinal cord injury. *Neurosci Bull, 29*(4), 436-444. doi:10.1007/s12264-013-1365-4

Lee, J. K., Geoffroy, C. G., Chan, A. F., Tolentino, K. E., Crawford, M. J., Leal, M. A., Kang, B., and Zheng, B. H. (2010). Assessing Spinal Axon Regeneration and Sprouting in Nogo-, MAG-, and OMgp-Deficient Mice. *Neuron, 66*(5), 663-670. doi:10.1016/j.neuron.2010.05.002

Lemons, M. L., Sandy, J. D., Anderson, D. K., and Howland, D. R. (2003). Intact aggrecan and chondroitin sulfate-depleted aggrecan core glycoprotein inhibit axon growth in the adult rat spinal cord. *Exp Neurol, 184*(2), 981-990. doi:10.1016/s0014-4886(03)00383-2

Li, C., Tropak, M. B., Gerlai, R., Clapoff, S., Abramow-Newerly, W., Trapp, B., Peterson, A., and Roder, J. (1994). Myelination in the absence of myelin-associated glycoprotein. *Nature, 369*(6483), 747-750. doi:10.1038/369747a0

Li, C. L., Li, K. C., Wu, D., Chen, Y., Luo, H., Zhao, J. R., Wang, S. S., Sun, M. M., Lu, Y. J., Zhong, Y. Q., Hu, X. Y., Hou, R., Zhou, B. B., Bao, L., Xiao, H. S., and Zhang, X. (2016). Somatosensory neuron types identified by high-coverage single-cell RNA-sequencing and functional heterogeneity. *Cell Res, 26*(8), 967. doi:10.1038/cr.2016.90

800 Li, M., Shibata, A., Li, C., Braun, P. E., McKerracher, L., Roder, J., Kater, S. B., and David, S.
801 (1996). Myelin-associated glycoprotein inhibits neurite/axon growth and causes growth
802 cone collapse. *J Neurosci Res, 46*(4), 404-414. doi:10.1002/(SICI)1097-
803 4547(19961115)46:4<404::AID-JNR2>3.0.CO;2-K [pii]10.1002/(SICI)1097-
804 4547(19961115)46:4<404::AID-JNR2>3.0.CO;2-K

805 Li, S., Xue, C., Yuan, Y., Zhang, R., Wang, Y., Wang, Y., Yu, B., Liu, J., Ding, F., Yang, Y.,
806 and Gu, X. (2015). The transcriptional landscape of dorsal root ganglia after sciatic nerve
807 transection. *Sci Rep, 5*, 16888. doi:10.1038/srep16888

808 Li, Y., Carlstedt, T., Berthold, C. H., and Raisman, G. (2004). Interaction of transplanted
809 olfactory-ensheathing cells and host astrocytic processes provides a bridge for axons to
810 regenerate across the dorsal root entry zone. *Exp Neurol, 188*(2), 300-308.
811 doi:10.1016/j.expneurol.2004.04.021

812 Lin, C. L., Heron, P., Hamann, S. R., and Smith, G. M. (2014). Functional distinction between
813 NGF-mediated plasticity and regeneration of nociceptive axons within the spinal cord.
814 *Neuroscience, 272*, 76-87. doi:10.1016/j.neuroscience.2014.04.053

815 Lindholm, T., Risling, M., Carlstedt, T., Hammarberg, H., Wallquist, W., Cullheim, S., and
816 Sköld, M. K. (2017). Expression of Semaphorins, Neuropilins, VEGF, and Tenascins in
817 Rat and Human Primary Sensory Neurons after a Dorsal Root Injury. *Front Neurol, 8*, 49.
818 doi:10.3389/fneur.2017.00049

819 Liu, S., Bohl, D., Blanchard, S., Bacci, J., Saïd, G., and Heard, J. M. (2009). Combination of
820 microsurgery and gene therapy for spinal dorsal root injury repair. *Mol Ther, 17*(6), 992-
821 1002. doi:10.1038/mt.2009.23

822 Liu, Y., Keefe, K., Tang, X., Lin, S., and Smith, G. M. (2014). Use of self-complementary
823 adeno-associated virus serotype 2 as a tracer for labeling axons: implications for axon
824 regeneration. *PLoS ONE, 9*(2), e87447. doi:10.1371/journal.pone.0087447

825 Liu, Y., Kelamangalath, L., Kim, H., Han, S. B., Tang, X., Zhai, J., Hong, J. W., Lin, S., Son, Y.
826 J., and Smith, G. M. (2016). NT-3 promotes proprioceptive axon regeneration when

827 combined with activation of the mTor intrinsic growth pathway but not with reduction of
828 myelin extrinsic inhibitors. *Exp Neurol, 283*(Pt A), 73-84.
829 doi:10.1016/j.expneurol.2016.05.021

830 Liuzzi, F. J., and Lasek, R. J. (1987). Astrocytes block axonal regeneration in mammals by
831 activating the physiological stop pathway. *Science, 237*(4815), 642-645.

832 Mar, F. M., Simões, A. R., Rodrigo, I. S., and Sousa, M. M. (2016). Inhibitory Injury Signaling
833 Represses Axon Regeneration After Dorsal Root Injury. *Mol Neurobiol, 53*(7), 4596-
834 4605. doi:10.1007/s12035-015-9397-6

835 Mason, M. R. J., Ehlert, E. M. E., Eggers, R., Pool, C. W., Hermening, S., Huseinovic, A.,
836 Timmermans, E., Blits, B., and Verhaagen, J. (2010). Comparison of AAV Serotypes for
837 Gene Delivery to Dorsal Root Ganglion Neurons. *Molecular Therapy, 18*(4), 715-724.
838 doi:10.1038/mt.2010.19

839 Montagutelli, X. (2000). Effect of the genetic background on the phenotype of mouse mutations.
840 *J Am Soc Nephrol, 11 Suppl 16*, S101-105.

841 Muir, E., De Winter, F., Verhaagen, J., and Fawcett, J. (2019). Recent advances in the
842 therapeutic uses of chondroitinase ABC. *Exp Neurol, 321*, 113032.
843 doi:10.1016/j.expneurol.2019.113032

844 Neumann, S., and Woolf, C. J. (1999). Regeneration of dorsal column fibers into and beyond the
845 lesion site following adult spinal cord injury. *Neuron, 23*(1), 83-91. doi:S0896-
846 6273(00)80755-2 [pii]

847 Nichols, E. L., and Smith, C. J. (2020). Functional Regeneration of the Sensory Root via Axonal
848 Invasion. *Cell Rep, 30*(1), 9-17.e13. doi:10.1016/j.celrep.2019.12.008

849 Niu, J., Ding, L., Li, J. J., Kim, H., Liu, J., Li, H., Moberly, A., Badea, T. C., Duncan, I. D., Son,
850 Y. J., Scherer, S. S., and Luo, W. (2013). Modality-based organization of ascending
851 somatosensory axons in the direct dorsal column pathway. *J Neurosci, 33*(45), 17691-
852 17709. doi:10.1523/JNEUROSCI.3429-13.2013

O'Donovan, K. J., Ma, K., Guo, H., Wang, C., Sun, F., Han, S. B., Kim, H., Wong, J. K., Charron, J., Zou, H., Son, Y. J., He, Z., and Zhong, J. (2014). B-RAF kinase drives developmental axon growth and promotes axon regeneration in the injured mature CNS. *J Exp Med, 211*(5), 801-814. doi:10.1084/jem.20131780

O'Shea, T. M., Burda, J. E., and Sofroniew, M. V. (2017). Cell biology of spinal cord injury and repair. *J Clin Invest, 127*(9), 3259-3270. doi:10.1172/jci90608

Ohtake, Y., Saito, A., and Li, S. (2018). Diverse functions of protein tyrosine phosphatase σ in the nervous and immune systems. *Exp Neurol, 302*, 196-204. doi:10.1016/j.expneurol.2018.01.014

Palmisano, I., Danzi, M. C., Hutson, T. H., Zhou, L., McLachlan, E., Serger, E., Shkura, K., Srivastava, P. K., Hervera, A., Neill, N. O., Liu, T., Dhrif, H., Wang, Z., Kubat, M., Wuchty, S., Merkenschlager, M., Levi, L., Elliott, E., Bixby, J. L., Lemmon, V. P., and Di Giovanni, S. (2019). Epigenomic signatures underpin the axonal regenerative ability of dorsal root ganglia sensory neurons. *Nat Neurosci, 22*(11), 1913-1924. doi:10.1038/s41593-019-0490-4

Peng, X., Zhou, Z., Hu, J., Fink, D. J., and Mata, M. (2010). Soluble Nogo receptor down-regulates expression of neuronal Nogo-A to enhance axonal regeneration. *J Biol Chem, 285*(4), 2783-2795. doi:10.1074/jbc.M109.046425

Quaglia, X., Beggah, A. T., Seidenbecher, C., and Zurn, A. D. (2008). Delayed priming promotes CNS regeneration post-rhizotomy in Neurocan and Brevican-deficient mice. *Brain, 131*(Pt 1), 240-249. doi:10.1093/brain/awm279

Ramer, M. S., Duraisingam, I., Priestley, J. V., and McMahon, S. B. (2001). Two-tiered inhibition of axon regeneration at the dorsal root entry zone. *The Journal of neuroscience : the official journal of the Society for Neuroscience, 21*(8), 2651-2660.

Ramer, M. S., Priestley, J. V., and McMahon, S. B. (2000). Functional regeneration of sensory axons into the adult spinal cord. *Nature, 403*(6767), 312-316. doi:10.1038/35002084

879 Smith, G. M., Falone, A. E., and Frank, E. (2012). Sensory axon regeneration: rebuilding
880 functional connections in the spinal cord. *Trends Neurosci, 35*(3), 156-163.
881 doi:10.1016/j.tins.2011.10.006

882 Son, Y. J. (2015). Synapsing with NG2 cells (polydendrocytes), unappreciated barrier to axon
883 regeneration? *Neural Regen Res, 10*(3), 346-348. doi:10.4103/1673-5374.153672

884 Steinmetz, M. P., Horn, K. P., Tom, V. J., Miller, J. H., Busch, S. A., Nair, D., Silver, D. J., and
885 Silver, J. (2005). Chronic enhancement of the intrinsic growth capacity of sensory
886 neurons combined with the degradation of inhibitory proteoglycans allows functional
887 regeneration of sensory axons through the dorsal root entry zone in the mammalian spinal
888 cord. *J Neurosci, 25*(35), 8066-8076. doi:10.1523/jneurosci.2111-05.2005

889 Stensaas, L. J., Partlow, L. M., Burgess, P. R., and Horch, K. W. (1987). Inhibition of
890 regeneration: the ultrastructure of reactive astrocytes and abortive axon terminals in the
891 transition zone of the dorsal root. *Prog Brain Res, 71*, 457-468. doi:10.1016/s0079-
892 6123(08)61846-4

893 Steward, O., Popovich, P. G., Dietrich, W. D., and Kleitman, N. (2012). Replication and
894 reproducibility in spinal cord injury research. *Exp Neurol, 233*(2), 597-605.
895 doi:10.1016/j.expneurol.2011.06.017

896 Steward, O., Zheng, B., and Tessier-Lavigne, M. (2003). False resurrections: distinguishing
897 regenerated from spared axons in the injured central nervous system. *J Comp Neurol,*
898 *459*(1), 1-8. doi:10.1002/cne.10593

899 Tan, C. L., Kwok, J. C., Patani, R., Ffrench-Constant, C., Chandran, S., and Fawcett, J. W.
900 (2011). Integrin activation promotes axon growth on inhibitory chondroitin sulfate
901 proteoglycans by enhancing integrin signaling. *J Neurosci, 31*(17), 6289-6295.
902 doi:10.1523/jneurosci.0008-11.2011

903 Tedeschi, A., Omura, T., and Costigan, M. (2017). CNS repair and axon regeneration: Using
904 genetic variation to determine mechanisms. *Exp Neurol, 287*(Pt 3), 409-422.
905 doi:10.1016/j.expneurol.2016.05.004

906 Tessler, A., Himes, B. T., Houle, J., and Reier, P. J. (1988). Regeneration of adult dorsal root
907 axons into transplants of embryonic spinal cord. *J Comp Neurol, 270*(4), 537-548.
908 doi:10.1002/cne.902700407

909 Thiede-Stan, N. K., and Schwab, M. E. (2015). Attractive and repulsive factors act through
910 multi-subunit receptor complexes to regulate nerve fiber growth. *J Cell Sci, 128*(14),
911 2403-2414. doi:10.1242/jcs.165555

912 Tom, V. J., Steinmetz, M. P., Miller, J. H., Doller, C. M., and Silver, J. (2004). Studies on the
913 development and behavior of the dystrophic growth cone, the hallmark of regeneration
914 failure, in an in vitro model of the glial scar and after spinal cord injury. *J Neurosci,*
915 *24*(29), 6531-6539. doi:10.1523/JNEUROSCI.0994-04.2004 24/29/6531 [pii]

916 Vargas, M. E., and Barres, B. A. (2007). Why is Wallerian degeneration in the CNS so slow?
917 *Annu Rev Neurosci, 30*, 153-179. doi:10.1146/annurev.neuro.30.051606.094354

918 Wang, R., King, T., Ossipov, M. H., Rossomando, A. J., Vanderah, T. W., Harvey, P., Cariani,
919 P., Frank, E., Sah, D. W., and Porreca, F. (2008). Persistent restoration of sensory
920 function by immediate or delayed systemic artemin after dorsal root injury. *Nat Neurosci,*
921 *11*(4), 488-496. doi:10.1038/nn2069

922 Wang, X., Hasan, O., Arzeno, A., Benowitz, L. I., Cafferty, W. B., and Strittmatter, S. M.
923 (2012). Axonal regeneration induced by blockade of glial inhibitors coupled with
924 activation of intrinsic neuronal growth pathways. *Exp Neurol, 237*(1), 55-69.
925 doi:10.1016/j.expneurol.2012.06.009

926 Wu, D., Klaw, M. C., Connors, T., Kholodilov, N., Burke, R. E., Côté, M. P., and Tom, V. J.
927 (2017). Combining Constitutively Active Rheb Expression and Chondroitinase Promotes
928 Functional Axonal Regeneration after Cervical Spinal Cord Injury. *Mol Ther, 25*(12),
929 2715-2726. doi:10.1016/j.ymthe.2017.08.011

930 Wu, D., Klaw, M. C., Kholodilov, N., Burke, R. E., Detloff, M. R., Côté, M. P., and Tom, V. J.
931 (2016). Expressing Constitutively Active Rheb in Adult Dorsal Root Ganglion Neurons
932 Enhances the Integration of Sensory Axons that Regenerate Across a Chondroitinase-

933 Treated Dorsal Root Entry Zone Following Dorsal Root Crush. *Front Mol Neurosci, 9*,
934 49. doi:10.3389/fnmol.2016.00049

935 Yao, M., Sun, H., Yuan, Q., Li, N., Li, H., Tang, Y., Leung, G. K., and Wu, W. (2019).
936 Targeting proteoglycan receptor PTPσ restores sensory function after spinal cord dorsal
937 root injury by activation of Erks/CREB signaling pathway. *Neuropharmacology, 144*,
938 208-218. doi:10.1016/j.neuropharm.2018.10.035

939 Yu, H., Fischer, G., Ferhatovic, L., Fan, F., Light, A. R., Weihrauch, D., Sapunar, D., Nakai, H.,
940 Park, F., and Hogan, Q. H. (2013). Intraganglionic AAV6 results in efficient and long-
941 term gene transfer to peripheral sensory nervous system in adult rats. *PLoS ONE, 8*(4),
942 e61266. doi:10.1371/journal.pone.0061266

943 Zhang, C., Jin, Y., Ziemba, K. S., Fletcher, A. M., Ghosh, B., Truit, E., Yurek, D. M., and Smith,
944 G. M. (2013). Long distance directional growth of dopaminergic axons along pathways
945 of netrin-1 and GDNF. *Exp Neurol, 250*, 156-164. doi:10.1016/j.expneurol.2013.09.022

946 Zhang, L., Ma, Z., Smith, G. M., Wen, X., Pressman, Y., Wood, P. M., and Xu, X. M. (2009a).
947 GDNF-enhanced axonal regeneration and myelination following spinal cord injury is
948 mediated by primary effects on neurons. *Glia, 57*(11), 1178-1191.
949 doi:10.1002/glia.20840

950 Zhang, L., Zheng, S., Wu, H., Wu, Y., Liu, S., Fan, M., and Zhang, J. (2009b). Identification of
951 BLyS (B lymphocyte stimulator), a non-myelin-associated protein, as a functional ligand
952 for Nogo-66 receptor. *J Neurosci, 29*(19), 6348-6352. doi:10.1523/jneurosci.5040-
953 08.2009

954 Zhang, Y., Zhang, X., Wu, D., Verhaagen, J., Richardson, P. M., Yeh, J., and Bo, X. (2007).
955 Lentiviral-mediated expression of polysialic acid in spinal cord and conditioning lesion
956 promote regeneration of sensory axons into spinal cord. *Mol Ther, 15*(10), 1796-1804.

957
958
959

960 **FIGURE LEGENDS**

961 **Figure 1. Intraganglionic AAV2-GFP labels proprioceptive and mechanoreceptive axons**

962 **(A)** Schematic illustration of intraganglionic injection of scAAV2-eGFP and a representative
963 DRG showing infected neurons expressing GFP at 2 weeks post-injection. **(B)** Mice expressing
964 GFP in >70% Nissl-stained neurons were used in the present study. **(C)** DRG transverse sections
965 showing GFP+ neurons (arrows) co-expressing neurofilament (NF), IB4, or CGRP. **(D)**
966 Quantitative comparisons of AAV2-GFP infected neurons illustrating preferential labeling of
967 large-diameter myelinated NF+ neurons, which mediate proprioception and mechanoreception.
968 n>20 sections, 3 mice. **(E)** A transverse section showing GFP+ axons along the root and within
969 the right side of the spinal cord, projecting into dorsal column, deeper laminae of the dorsal horn
970 and into the ventral horn. An arrow denotes superficial laminae I-IIi lacking GFP fluorescence.
971 **(E', E")** Enlarged views of the superficial dorsal horn, illustrating lack of GFP-fluorescence
972 where CGRP+ nociceptive axons (magenta) innervate. DH, dorsal horn; DR, dorsal root; VH;
973 ventral horn. Scale bars=50μm **(A, C, E', E")**, 200μm **(E)**.
974
975 **Figure 2. Additional strategies for complete lesions and evaluation of DR regeneration**
976 DR regeneration in adult wildtype mice assessed in wholemounts (**A-D**) and transverse sections
977 (**E, F**) 2 weeks after L4 and L5 DR crush. **(A)** Schematic illustration of crushing roots prior to
978 intraganglionic AAV2-GFP injections to avoid labeling of degenerating distal stump axons. **(B)**
979 Wholemount view of completely crushed L4 and L5 DRs illustrating hundreds of GFP+ axons
980 terminated at the entrance of spinal cord. **(B', B")** Enlarged views illustrating most axons
981 terminated near the border. **(C-C")** Wholemount views of incompletely crushed DRs showing
982 spared axons with long intraspinal projections. Spared axons are easily detectable in
983 wholemounts and commonly observed in the outermost dorsal rootlets (arrows). **(D)**
984 Wholemount view of L4 DREZ illustrating GFP+ axons that crossed the astrocyte:PNS border
985 (dotted line) and terminated nearby. The astrocytic border is identified by GFAP immunostaining
986 of astrocytes (red). Yellow line denotes spinal cord midline recognized by the midline vein. **(E)**
987 Four-color immunolabeling of transverse sections illustrating limited penetration of GFP+ or
988 CGRP+ axons through the DREZ. White dotted lines approximate the peripheral border of the
989 DREZ (astrocyte:PNS border) by locating peripherally projecting astrocytic processes (red) or by
990 greater abundance of cell nuclei in the PNS (blue). Axons rarely extended >200μm beyond the

991 border. Arrowheads denote frequently observed axons that grew along the growth-permissive
992 dura. Arrow denotes occasionally observed subdural axons located several hundred microns past
993 the border. **(F)** Quantitative analysis of DR regeneration on transverse sections (13 sections, 3
994 mice). ~90% GFP+ axons terminated within ~100μm of the border. Axons growing farther than
995 100μm are considered as having penetrated the DREZ. DH, dorsal horn; DR, dorsal root; S.C.,
996 spinal cord. Scale bars=200μm **(B-B", C-C", D, E)**.
997
998 **Figure 3. Genetic deletion of Nogo/MAG/OMgp elicits little intraspinal regeneration**
999 DR regeneration in Nogo/MAG/OMgp tKO mice assessed in wholemounts (**C**) or transverse
1000 sections (**D, F**) 2 weeks after L4 and L5 DR crush. **(A)** Identification of triple null mutants (red)
1001 lacking Nogo (A, B, C), MAG and OMgp. **(B)** Schematic illustration of the experimental
1002 procedures. **(C)** Wholemount views of L4-L5 DREZ illustrating termination of hundreds of
1003 GFP+ axons near the astrocyte:PNS border (dotted line), as in wildtype mice. The astrocytic
1004 border is identified by GFAP immunostaining of astrocytes (red). **(C', C")** Enlarged views of L4
1005 and L5 DREZ in (**C**). Arrows denote axons extending longer processes past the DREZ, which
1006 were also frequently observed in wildtype mice. **(D)** Representative transverse sections
1007 illustrating little if any enhanced regeneration of GFP+ axons across the DREZ. Arrows denote
1008 axons that grew dorsally along the pia matter, as also observed in wildtype mice. **(E)**
1009 Quantitative comparisons illustrating no significant difference in WT and Nogo/MAG/OMgp
1010 tKO mice. 100μm, p=0.9738, df=162; 200μm, p=0.5046, df=162; 300μm, p=0.1454, df=162.
1011 Two-way repeated-measures ANOVA with Sidak's multiple comparisons test (WT: 13 sections,
1012 3 mice; tKO: 16 sections, 5 mice). S.C., spinal cord; ns, not significant. Scale bars=200μm (**C-**
1013 **C", D-D"**).
1014
1015 **Figure 4. Additional CSPG removal enables minimal intraspinal regeneration in tKO**
1016 **myelin mutants**
1017 DR regeneration in ChABC-expressed Nogo/MAG/OMgp tKO mice assessed in wholemounts
1018 (**B**) and transverse sections (**D, C**) 2 weeks after L4 and L5 DR crush. **(A)** Schematic illustration
1019 of the experimental procedures. LV-ChABC was injected into ipsilateral dorsal horn at multiple
1020 locations rostrocaudally along the L4-L5 DREZ. **(B)** Wholemount views of a ChABC-expressed
1021 tKO showing hundreds of GFP+ axons in L4 and L5 roots terminated near the astrocyte:PNS

border (dotted line), as in WT and tKO mice. The astrocytic border is identified by GFAP immunostaining of astrocytes (red). **(C)** Representative transverse sections illustrating effective degradation of CSPGs and modestly enhanced intraspinal regeneration. CS-56 immunoreactivity is very low in ipsilateral dorsal horn (asterisks), indicating effective removal of inhibitory GAG chains of CSPGs. Arrowheads denote Schwann cell-associated CS-56 immunoreactivity, which is markedly reduced but discernable in ChABC-expressed tKO. **(C')** Enlarged views showing a few GFP+ axons that penetrated the DREZ and are located at the top of the dorsal horn (arrows); such axons were not observed in WT or Nogo/MAG/OMgp tKO mice. **(D)** Quantitative comparisons illustrating modestly improved regeneration in ChABC-expressed Nogo/MAG/OMgp tKO mice: ~15% GFP+ penetrated the DREZ and remained within ~200µm of the border. ChABC-expressed tKO vs. WT: 100µm, **p=0.0022, df=186; 200µm, ***p=0.0003, df=186; 300µm, p=0.4818, df=186. ChABC-expressed tKO vs. tKO: 100µm, **p=0.0086, df=186; 200µm, **p=0.0099, df=186; 300µm, p=0.9262, df=186. Two-way repeated-measures ANOVA with Sidak's multiple comparisons test (WT: 13 sections, 3 mice; tKO: 16 sections, 5 mice; ChABC-tKO: 14 sections, 3 mice). S.C., spinal cord; ns, not significant. Scale bars=200µm (**B, C, C'**).

Figure 5. Chronic regeneration failure at the DREZ lacking Nogo/MAG/OMgp and CSPGs

DR regeneration in WT (**A-D**), Nogo/MAG/OMgp tKO (**E-G**), and ChABC-expressed Nogo/MAG/OMgp tKO mice (**H-K**) analyzed 4 weeks after L4 and L5 DR crush. **(A)** Schematic illustration of the experimental procedures. **(B)** Wholemount view of L5 DREZ in a WT mouse showing no noticeably enhanced regeneration into the spinal cord. **(C, C')** Transverse sections showing no improved penetration of GFP+ (green) and CGRP+ axons (magenta) through the DREZ. **(D)** Quantitative comparisons of WT mice at 2wpi and 4wpi illustrating no significant difference. 100µm, p=0.5292, df=102. Two-way repeated-measured ANOVA with Sidak's multiple comparisons test (WT-2wpi: 13 sections, 3 mice; WT-4wpi: 14 sections, 4 mice). **(E)** Wholemount view of L4-L5 DREZ in a tKO showing no marked increase in intraspinal regeneration. **(F, F')** Transverse sections of a tKO mouse showing GFP+ (green) and CGRP+ axons (magenta) remaining at the DREZ at 4 wpi. **(G)** Quantitative comparisons of tKO mice at 2wpi and 4wpi illustrating no significant difference. 100µm, p=0.5067, df=168; 200µm, p>0.9999, df=168; 300µm, p>0.9999, df=168. Two-way repeated-measures ANOVA with

Sidak's multiple comparisons test (tKO-2wpi: 16 sections, 5 mice; tKO-4wpi: 14 sections, 5 mice). **(H)** Wholemount view of L4-L5 DREZ in a ChABC-expressed tKO showing no noticeably enhanced intraspinal regeneration. **(I. I')** Transverse sections of a ChABC-expressed tKO showing GFP+ (green) and CGRP+ axons (magenta) remaining at the DREZ at 4wpi. **(J)** Quantitative comparisons of ChABC-expressed tKO mice at 2wpi and 4wpi illustrating no significant increase in GFP+ axons that penetrated the DREZ. 100µm, p=0.0027, df=60; 200µm, p=0.936, df=60; 300µm, p>0.9999, df=60. Two-way repeated-measures ANOVA with Sidak's multiple comparisons test (ChABC-tKO-2wpi: 14 sections, 3 mice; ChABC-tKO-4wpi: 12 sections, 3 mice). **(K)** Quantitative comparisons of WT, tKO and ChABC-expressed tKO at 4wpi showing no significant difference in GFP+ axons crossing the DREZ. ChABC-expressed tKO vs. WT: 100µm, ***p=0.0001, df=144; 200µm, p=0.668, df=144; 300µm, p=0.7582, df=144). Two-way repeated-measures ANOVA with Sidak's multiple comparisons test. Scale bars=200µm (**B, C-C', E-F', H-I'**).

Figure 6. Conditioned DR axons do not penetrate the DREZ lacking Nogo/MAG/OMgp

(A) Schematic illustration of the experimental procedures. Nogo/MAG/OMgp tKO mice received a nerve conditioning lesion 10 days before L4 and L5 DR crush and were assessed at 2wpi. **(B)** Wholemount view of a conditioned tKO showing hundreds of GFP+ axons terminated near the astrocyte:PNS border (dotted line), as in WT and tKO mice. **(C, C')** Transverse sections of a conditioned tKO illustrating little if any enhanced regeneration of GFP+ (green) or CGRP+ axons (magenta) across the DREZ. An arrow denotes occasionally observed GFP+ axons that reached dorsolateral grey matter. **(D)** Quantitative comparisons illustrating no significant difference in WT, tKO and conditioned tKO mice. tKO vs. conditioned tKO: 100µm, ****p < 0.0001, df=220; 200µm, p = 0.9991, df=220; 300µm, p > 0.9999, df=220. Two-way repeated-measures ANOVA with Sidak's multiple comparisons test (WT: 13 sections, 3 mice; tKO: 16 sections, 5 mice; conditioned-tKO: 11 sections, 3 mice). ns, not significant. Scale bars=200µm (**B, C, C'**).

Figure 7. Additional CSPG removal does not enhance penetration in conditioned tKO mice

(A) Schematic illustration of the experimental procedures. LV-ChABC was injected into Nogo/MAG/OMgp tKO mice that received a conditioning lesion 10 days before L4 and L5 DR

crush. **(B)** Wholemount view of a ChABC/conditioned tKO showing hundreds of GFP+ axons that remain near the border (dotted line). **(C-C')** Transverse sections of a ChABC/conditioned tKO illustrating effective CSPG degradation confirmed by the lack of CS-56 immunoreactivity (asterisks) and little if any intraspinal regeneration of GFP+ axons. **(D-D')** Additional transverse sections of a ChABC/conditioned tKO illustrating limited intraspinal regeneration of GFP+ or CGRP+ axons (magenta). Arrows denote occasionally observed GFP+ axons that enter dorsal grey matter. **(E)** Quantitative comparisons illustrating no significant difference in ChABC/conditioned tKO and conditioned tKO mice. 100µm, p=0.7629, df=114; 200µm, p=0. 2671, df=114. Two-way repeated-measures ANOVA with Sidak's multiple comparisons test (conditioned tKO: 11 sections, 3 mice; ChABC/conditioned tKO: 10 sections, 4 mice). **(F)** Quantitative summary illustrating minimal intraspinal regeneration of even conditioned axons after concurrent removal of myelin inhibitors and CSPGs; Only ~10% GFP+ axons extended ~100um past the DREZ. 100µm, *p=0.0488, df=300 (WT vs ChABC expressed tKO), ****p<0.0001, df=300 (WT vs conditioned tKO, WT vs ChABC/conditioned tKO); 200µm, *p=0.014, df = 300 (WT vs ChABC expressed tKO, **p=0.0024, df = 300 (WT vs ChABC/conditioned tKO); 300 µm, p>0.9999; df = 300. Two-way repeated-measures ANOVA with Sidak's multiple comparisons test. Scale bars=200µm (**B, C, C', D, D'**).

Figure 8. Nogo/MAG/OMgp removal markedly enhances GDNF-induced intraspinal regeneration

GDNF-induced intraspinal regeneration analyzed in WT (**A-D**) and Nogo/MAG/OMgp tKO mice (**E-G'**) 2 weeks after L4 and L5 DR crush. **(A)** Schematic illustration showing intraspinal injections of LV-GDNF at the time of root crush and AAV2-GFP injections in WT mice. **(B)** Wholemount view of a GDNF-expressed WT illustrating hundreds of GFP+ axons largely remaining near the border. **(C-C')** Transverse sections of a GDNF-expressed WT showing a number of GFP+ (green) or CGRP+ axons (magenta) that cross the DREZ and extend further into the dorsal funiculus and grey matter. **(D)** Quantitative comparisons illustrating significantly enhanced penetration of GFP+ axons across the DREZ. 100µm, 200µm and 300µm, ****p<0.0001, df=156; 400µm, p=0.2446, df=156. Two-way repeated-measures ANOVA with Sidak's multiple comparisons test (WT: 13 sections, 3 mice; GDNF-expressed WT: 15 sections, 3 mice). **(E)** Schematic illustration of the experimental procedures in Nogo/MAG/OMgp tKO

mice. **(F)** Wholemount view of a GDNF-expressed tKO mouse revealing intensely fluorescent area of the L4 and L5 DREZ (arrows), likely due to densely accumulated subdural GFP+ axons. **(G-G')** Transverse sections of a GDNF-expressed tKO mouse displaying numerous GFP+ axons regenerating deep into dorsal horn. Asterisks denote CGRP immunoreactivity in deep dorsal laminae (magenta), presumably indicating enhanced regeneration of CGRP+ axons in GDNF-expressed tKO, as compared to that in GDNF-expressed WT. **(H)** Quantitative comparisons illustrating markedly greater intraspinal growth of GFAP-labeled axons in GDNF-expressed tKO than in GDNF-expressed WT mice. 100μm and 200μm, ****p<0.0001, df=174; 300μm, *p=0.028, df=174; 400μm, p=0.9975, df=174. Two-way repeated-measures ANOVA with Sidak's multiple comparisons test (GDNF-expressed WT: 15 sections, 3 mice; GDNF-expressed tKO: 16 sections, 5 mice). ns, not significant. Scale bars=200μm (**B, C, C', F, G, G'**).

Figure 9. CSPG removal further enhances GDNF-induced intraspinal regeneration in Nogo/MAG/OMgp tKO mice

(A) Schematic illustration of the experimental procedures. LV-ChABC and LV-GDNF were injected into dorsal horn along the L4-L5 DREZ in Nogo/MAG/OMgp tKO mice. **(B)** Wholemount view of a ChABC/GDNF-expressed tKO showing broader areas of the DREZ and the CNS with densely accumulated GFP+ axons (arrows). Arrowheads denote numerous axons extending rostrocaudally close to the midline. **(C-C')** Transverse sections of a ChABC/GDNF-expressed tKO showing effective degradation of CSPGs confirmed by CS-56 immunoreactivity and many GFP+ axons densely filling broad and deep areas of the dorsal horn. **(D)** Transverse sections of a ChABC/GDNF-expressed tKO showing enhanced intraspinal regeneration of GFP+ axons and CGRP+ axons (magenta). CGRP+ immunoreactivity is bright, dense and remarkably restricted to the superficial laminae. **(E)** Quantitative comparisons illustrating significantly more GFP+ axons in deeper portions of the dorsal horn in ChABC/GDNF-expressed tKO. 100μm, p=0.5389, df=210; 200μm, p=0.9891, df=210; 300μm, p=0.2358, df=210; 400μm, p=0.0074, df=210; 500μm, p=0.5805, df=210. Two-way repeated-measures ANOVA with Sidak's multiple comparisons test (ChABC/GDNF-expressed tKO: 19 sections, 8 mice; GDNF-expressed tKO: 16 sections, 5 mice). ns, not significant. Scale bars=200μm (**B, C, C', D**).

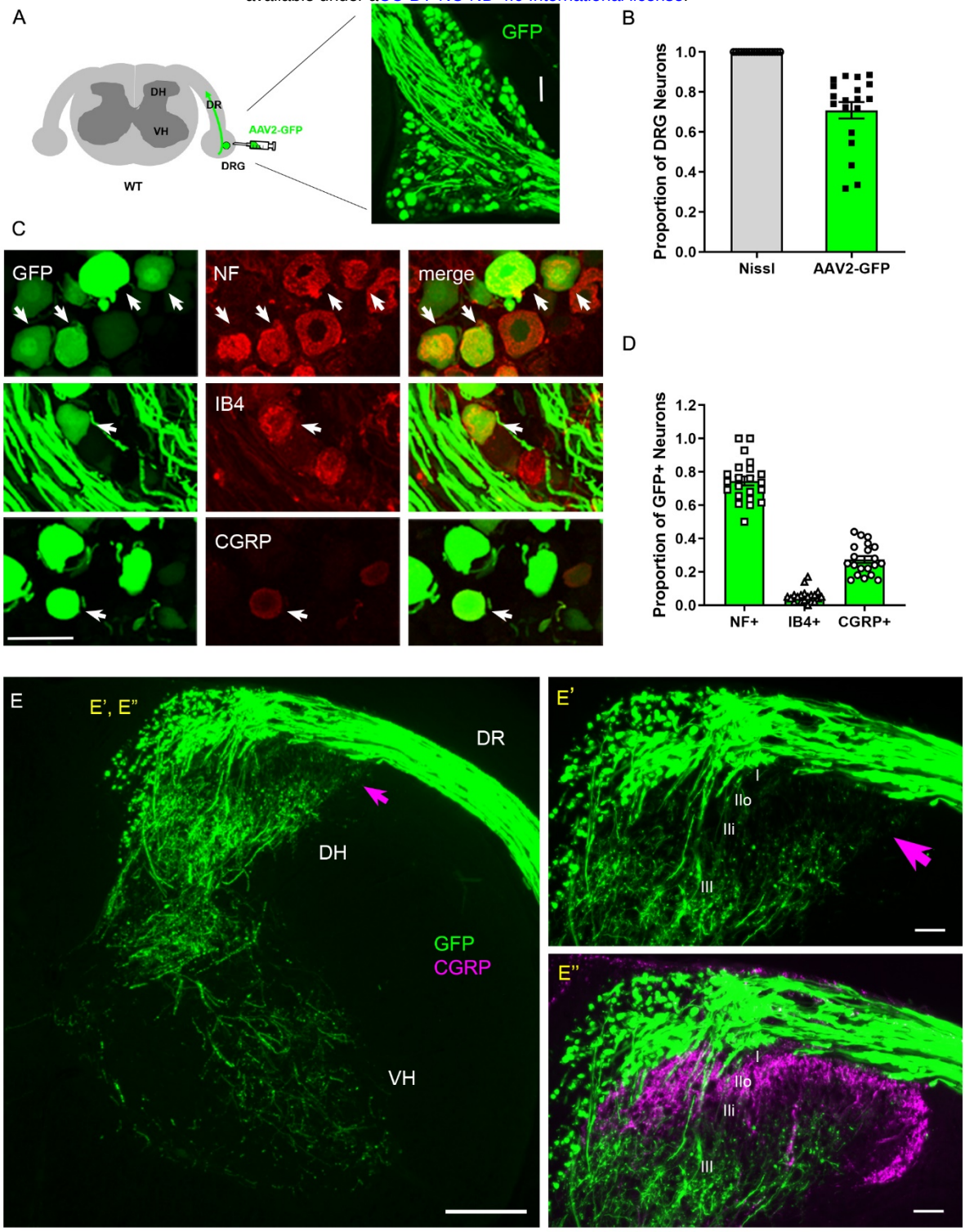

Figure 1. Intraganglionic AAV2-GFP labels proprioceptive and mechanoreceptive axons
(A) Schematic illustration of intraganglionic injection of scAAV2-eGFP and a representative DRG showing infected neurons expressing GFP at 2 weeks post-injection. **(B)** Mice expressing GFP in >70% Nissl-stained neurons were used in the present study. **(C)** DRG transverse sections showing GFP+ neurons (arrows) co-expressing neurofilament (NF), IB4, or CGRP. **(D)** Quantitative comparisons of AAV2-GFP infected neurons illustrating preferential labeling of large-diameter myelinated NF+ neurons, which mediate proprioception and mechanoreception. n>20 sections, 3 mice. **(E)** A transverse section showing GFP+ axons along the root and within the right side of the spinal cord, projecting into dorsal column, deeper laminae of the dorsal horn and into the ventral horn. An arrow denotes superficial laminae I-IIi lacking GFP fluorescence. **(E', E")** Enlarged views of the superficial dorsal horn, illustrating lack of GFP-fluorescence where CGRP+ nociceptive axons (magenta) innervate. DH, dorsal horn; DR, dorsal root; VH; ventral horn. Scale bars=50µm **(A, C, E', E")**, 200µm **(E)**.

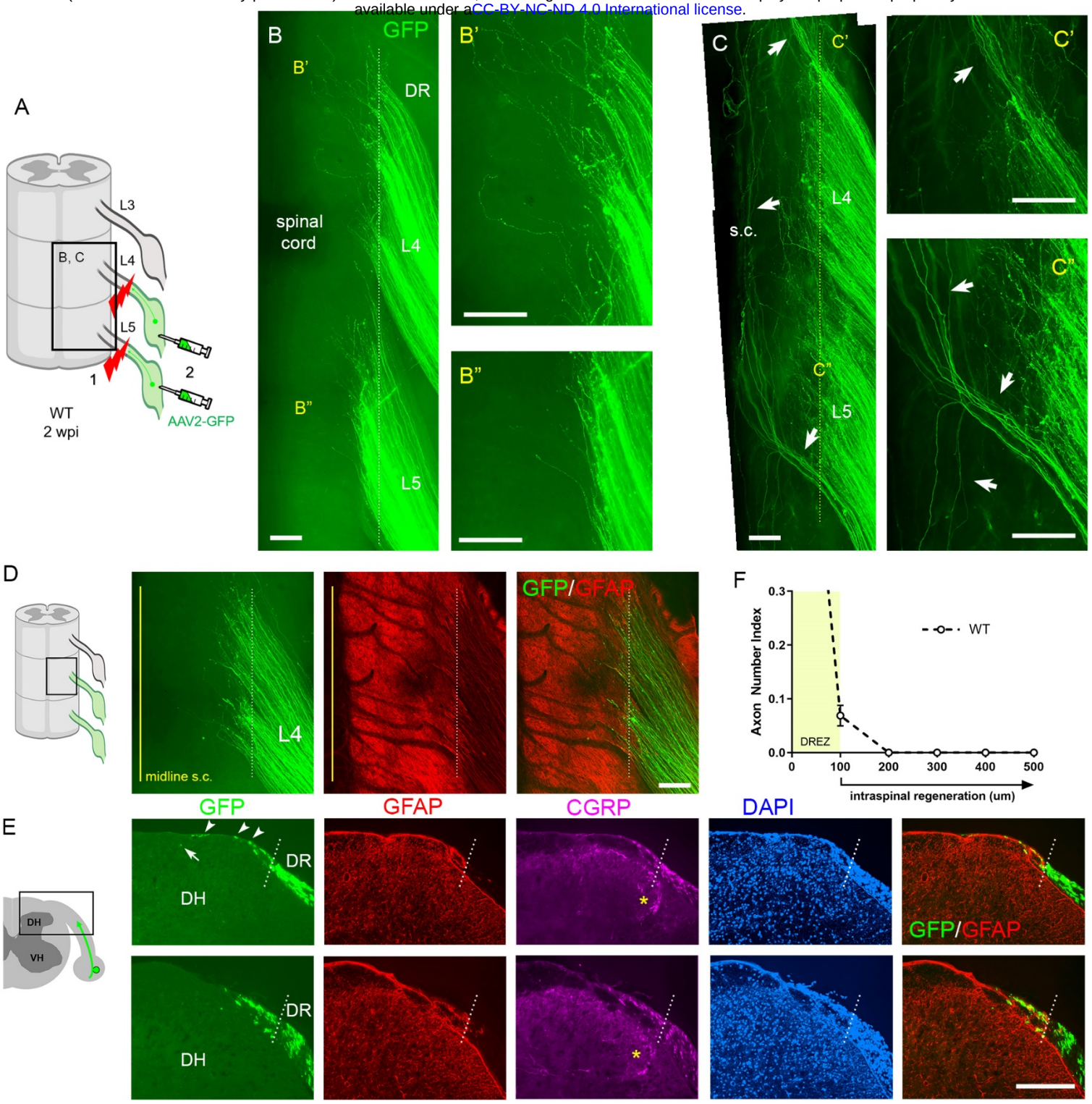

Figure 2. Additional strategies for complete lesions and evaluation of DR regeneration

DR regeneration in adult wildtype mice assessed in wholemounts (**A-D**) and transverse sections (**E, F**) 2 weeks after L4 and L5 DR crush. **(A)** Schematic illustration of crushing roots prior to intraganglionic AAV2-GFP injections to avoid labeling of degenerating distal stump axons. **(B)** Wholemount view of completely crushed L4 and L5 DRs illustrating hundreds of GFP+ axons terminated at the entrance of spinal cord. **(B', B")** Enlarged views illustrating most axons terminated near the border. **(C-C")** Wholemount views of incompletely crushed DRs showing spared axons with long intraspinal projections. Spared axons are easily detectable in wholemounts and commonly observed in the outermost dorsal rootlets (arrows). **(D)** Wholemount view of L4 DREZ illustrating GFP+ axons that crossed the astrocyte:PNS border (dotted line) and terminated nearby. The astrocytic border is identified by GFAP immunostaining of astrocytes (red). Yellow line denotes spinal cord midline recognized by the midline vein. **(E)** Four-color immunolabeling of transverse sections illustrating limited penetration of GFP+ or CGRP+ axons through the DREZ. White dotted lines

approximate the peripheral border of the DREZ (astrocyte:PNS border), by locating peripherally projecting astrocytic processes (red) or by greater abundance of cell nuclei in the PNS (blue). Axons rarely extended >200µm beyond the border. Arrowheads denote frequently observed axons that grew along the growth-permissive dura. Arrow denotes occasionally observed subdural axons located several hundred microns past the border. **(F)** Quantitative analysis of DR regeneration on transverse sections (13 sections, 3 mice). ~90% GFP+ axons terminated within ~100µm of the border. Axons growing farther than 100µm are considered as having penetrated the DREZ. DH, dorsal horn; DR, dorsal root; S.C., spinal cord. Scale bars=200µm **(B-B", C-C", D, E)**.

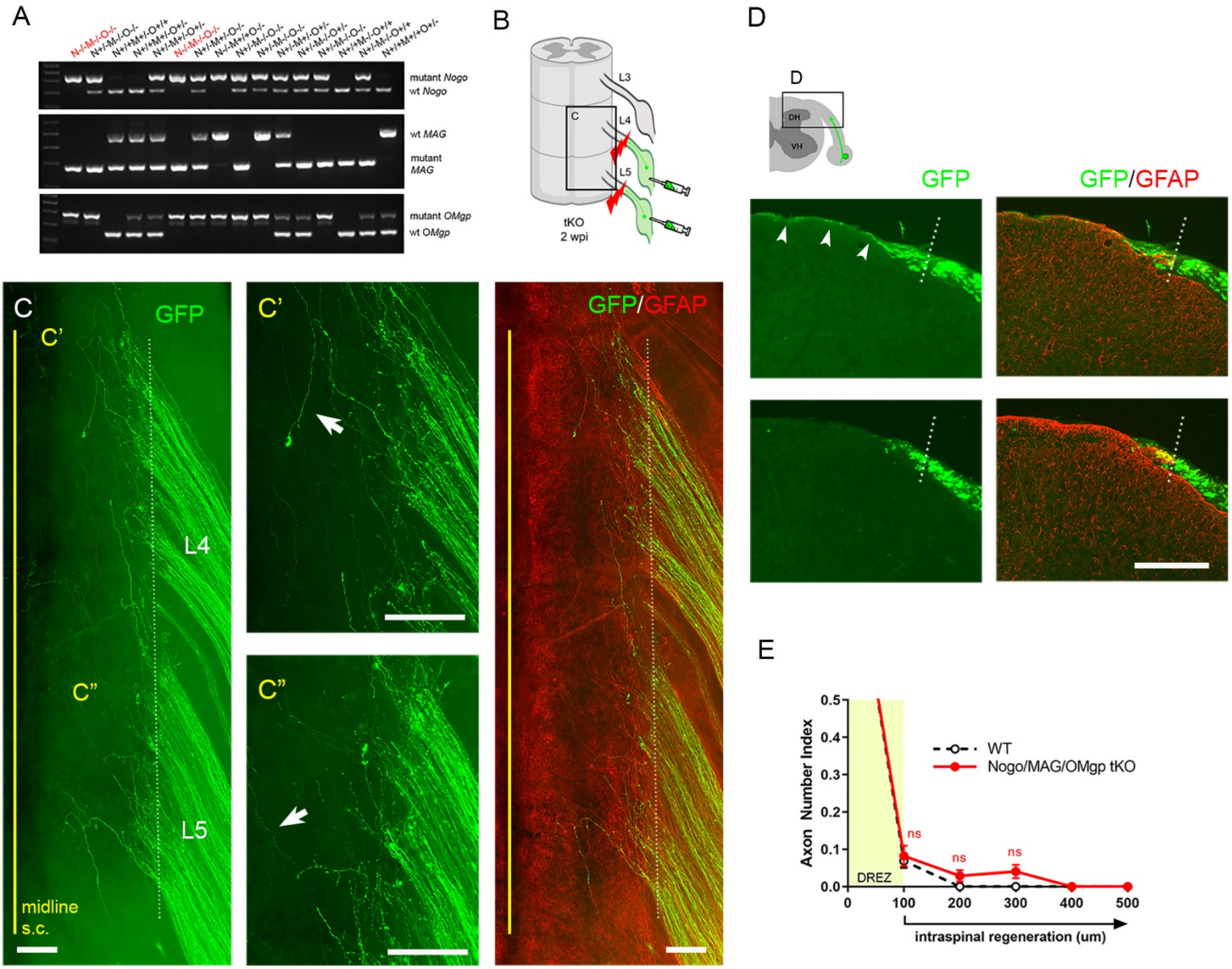

Figure 3. Genetic deletion of Nogo/MAG/OMgp elicits little intraspinal regeneration

DR regeneration in Nogo/MAG/OMgp tKO mice assessed in wholemounts (**C**) or transverse sections (**D, F**) 2 weeks after L4 and L5 DR crush. **(A)** Identification of triple null mutants (red) lacking Nogo (A, B, C), MAG and OMgp. **(B)** Schematic illustration of the experimental procedures. **(C)** Wholemount views of L4-L5 DREZ illustrating termination of hundreds of GFP+ axons near the astrocyte:PNS border (dotted line), as in wildtype mice. The astrocytic border is identified by GFAP immunostaining of astrocytes (red). **(C', C")** Enlarged views of L4 and L5 DREZ in (**C**). Arrows denote axons extending longer processes past the DREZ, which were also frequently observed in wildtype mice. **(D)** Representative transverse sections illustrating little if any enhanced regeneration of GFP+ axons across the DREZ. Arrows denote axons that grew dorsally along the pia matter, as also observed in wildtype mice. **(E)** Quantitative comparisons illustrating no significant difference in WT and Nogo/MAG/OMgp tKO mice. 100µm, p=0.9738, df=162; 200µm, p=0.5046, df=162; 300µm, p=0.1454, df=162. Two-way repeated-measures ANOVA with Sidak's multiple comparisons test (WT: 13 sections, 3 mice; tKO: 16 sections, 5 mice). S.C., spinal cord; ns, not significant. Scale bars=200µm (**C-C", D-D"**).

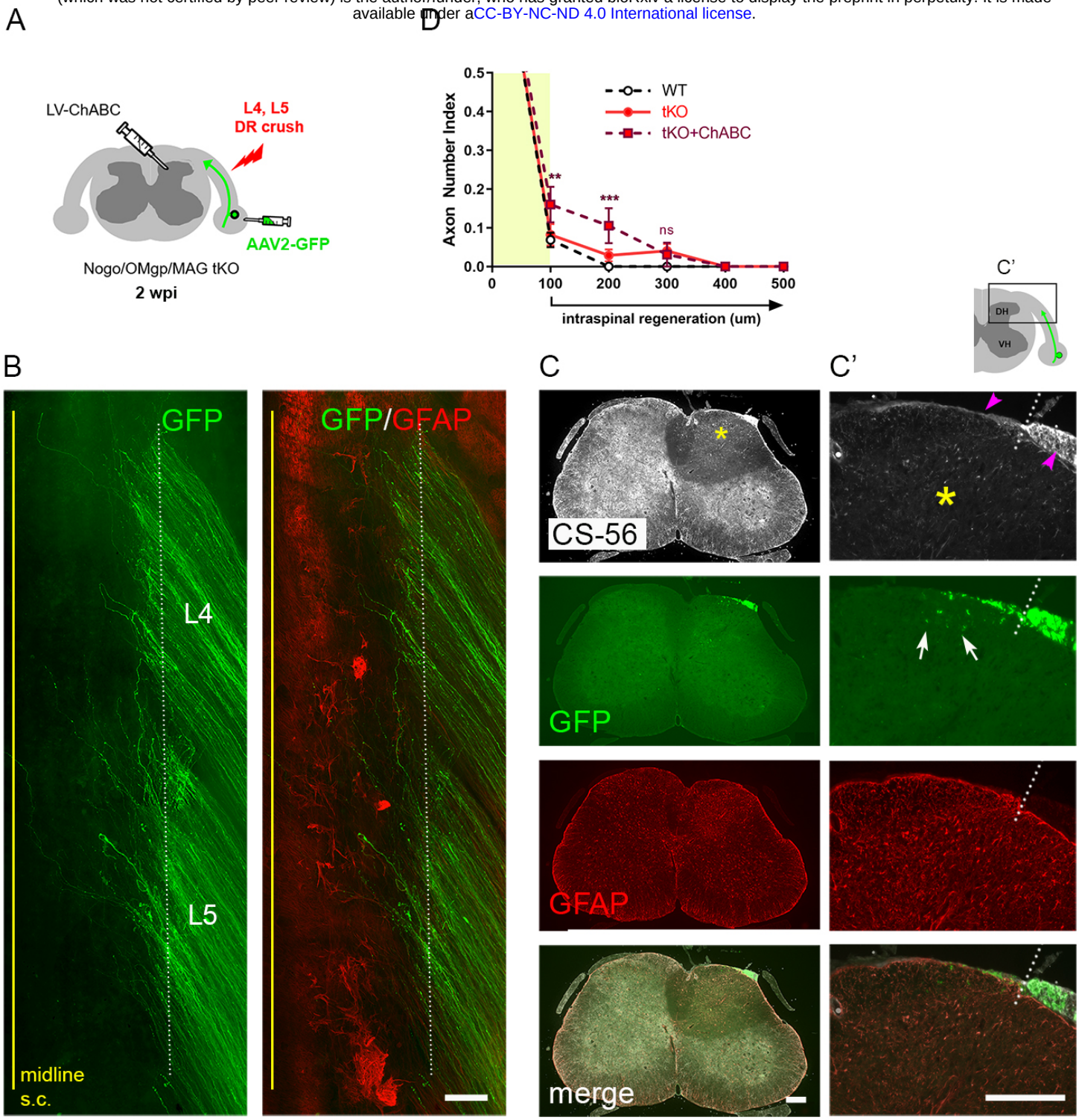

Figure 4. Additional CSPG removal enables minimal intraspinal regeneration in tKO myelin mutants

DR regeneration in ChABC-expressed Nogo/MAG/OMgp tKO mice assessed in wholemounts (**B**) and transverse sections (**D, C**) 2 weeks after L4 and L5 DR crush. **(A)** Schematic illustration of the experimental procedures. LV-ChABC was injected into ipsilateral dorsal horn at multiple locations rostrocaudally along the L4-L5 DREZ. **(B)** Wholemount views of a ChABC-expressed tKO showing hundreds of GFP+ axons in L4 and L5 roots terminated near the astrocyte:PNS border (dotted line), as in WT and tKO mice. The astrocytic border is identified by GFAP immunostaining of astrocytes (red). **(C)** Representative transverse sections illustrating effective degradation of CSPGs and modestly enhanced intraspinal regeneration. CS-56 immunoreactivity is very low in ipsilateral dorsal horn (asterisks), indicating effective removal of inhibitory GAG chains of CSPGs. Arrowheads denote Schwann cell-associated CS-56 immunoreactivity, which is markedly reduced but discernable in ChABC-expressed tKO. **(C')** Enlarged views showing a few GFP+ axons that penetrated the DREZ and are located at the top of the dorsal horn (arrows); such axons were not observed in WT or Nogo/MAG/OMgp tKO mice. **(D)** Quantitative comparisons illustrating modestly improved regeneration in ChABC-expressed Nogo/MAG/OMgp tKO mice: ~15% GFP+ penetrated the DREZ and remained within ~200μm of the border. ChABC-expressed tKO vs. WT: 100μm, **p=0.0022, df=186; 200μm, ***p=0.0003, df=186; 300μm, p=0.4818, df=186. ChABC-expressed tKO vs. tKO: 100μm, **p=0.0086, df=186; 200μm, **p=0.0099, df=186; 300μm, p=0.9262, df=186. Two-way repeated-measures ANOVA with Sidak's multiple comparisons test (WT: 13 sections, 3 mice; tKO: 16 sections, 5 mice; ChABC-tKO: 14 sections, 3 mice). S.C., spinal cord; ns, not significant. Scale bars=200μm (**B, C, C'**).

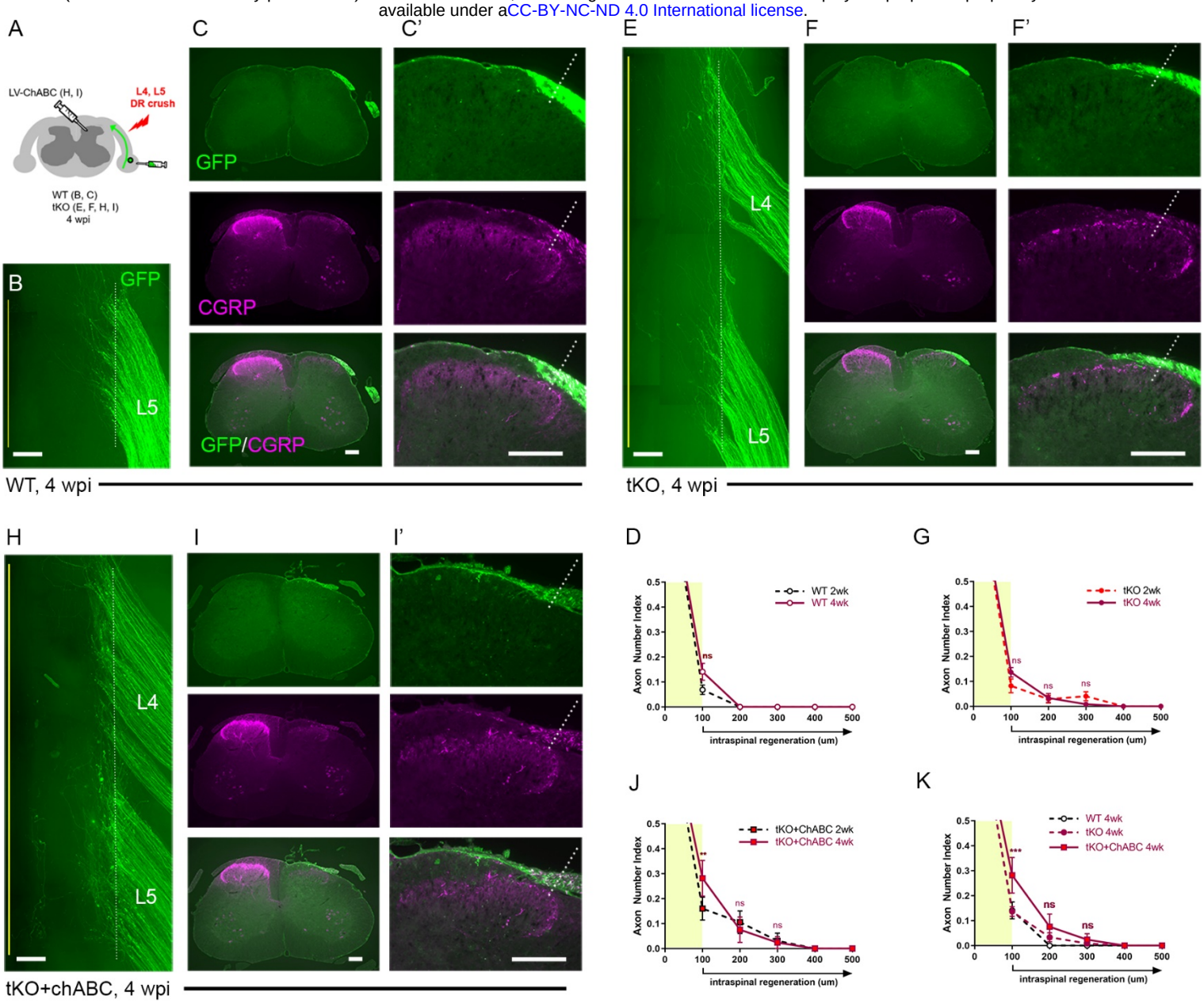

Figure 5. Chronic regeneration failure at the DREZ lacking Nogo/MAG/OMgp and CSPGs

DR regeneration in WT (**A-D**), Nogo/MAG/OMgp tKO (**E-G**), and ChABC-expressed Nogo/MAG/OMgp tKO mice (**H-K**) analyzed 4 weeks after L4 and L5 DR crush. **(A)** Schematic illustration of the experimental procedures. **(B)** Wholemount view of L5 DREZ in a WT mouse showing no noticeably enhanced regeneration into the spinal cord. **(C, C')** Transverse sections showing no improved penetration of GFP+ (green) and CGRP+ axons (magenta) through the DREZ. **(D)** Quantitative comparisons of WT mice at 2wpi and 4wpi illustrating no significant difference. 100µm, p=0.5292, df=102. Two-way repeated-measured ANOVA with Sidak's multiple comparisons test (WT-2wpi: 13 sections, 3 mice; WT-4wpi: 14 sections, 4 mice). **(E)** Wholemount view of L4-L5 DREZ in a tKO showing no marked increase in intraspinal regeneration. **(F, F')** Transverse sections of a tKO mouse showing GFP+ (green) and CGRP+ axons (magenta) remaining at the DREZ at 4 wpi. **(G)** Quantitative comparisons of tKO mice at 2wpi and 4wpi illustrating no significant difference. 100µm, p=0.5067, df=168; 200µm, p>0.9999, df=168; 300µm, p>0.9999, df=168. Two-way repeated-measures ANOVA with Sidak's multiple comparisons test (tKO-2wpi: 16 sections, 5 mice; tKO-4wpi: 14 sections, 5 mice). **(H)** Wholemount view of L4-L5 DREZ in a ChABC-expressed tKO showing no noticeably enhanced intraspinal regeneration. **(I. I')** Transverse sections of a ChABC-expressed tKO showing GFP+ (green) and CGRP+ axons (magenta) remaining at the DREZ at 4wpi. **(J)** Quantitative comparisons of ChABC-expressed tKO mice at 2wpi and 4wpi illustrating no significant increase in GFP+ axons that penetrated the DREZ. 100µm, p=0.0027, df=60; 200µm, p=0.936, df=60; 300µm, p>0.9999, df=60. Two-way repeated-measures ANOVA with Sidak's multiple comparisons test (ChABC-tKO-2wpi: 14 sections, 3 mice; ChABC-tKO-4wpi: 12 sections, 3 mice). **(K)** Quantitative comparisons of WT, tKO and ChABC-expressed tKO at 4wpi showing no significant difference in GFP+ axons crossing the DREZ. ChABC-expressed tKO vs. WT: 100µm, ***p=0.0001, df=144; 200µm, p=0.668, df=144; 300µm, p=0.7582, df=144). Two-way repeated-measures ANOVA with Sidak's multiple comparisons test. Scale bars=200µm (**B, C-C', E-F', H-I'**).

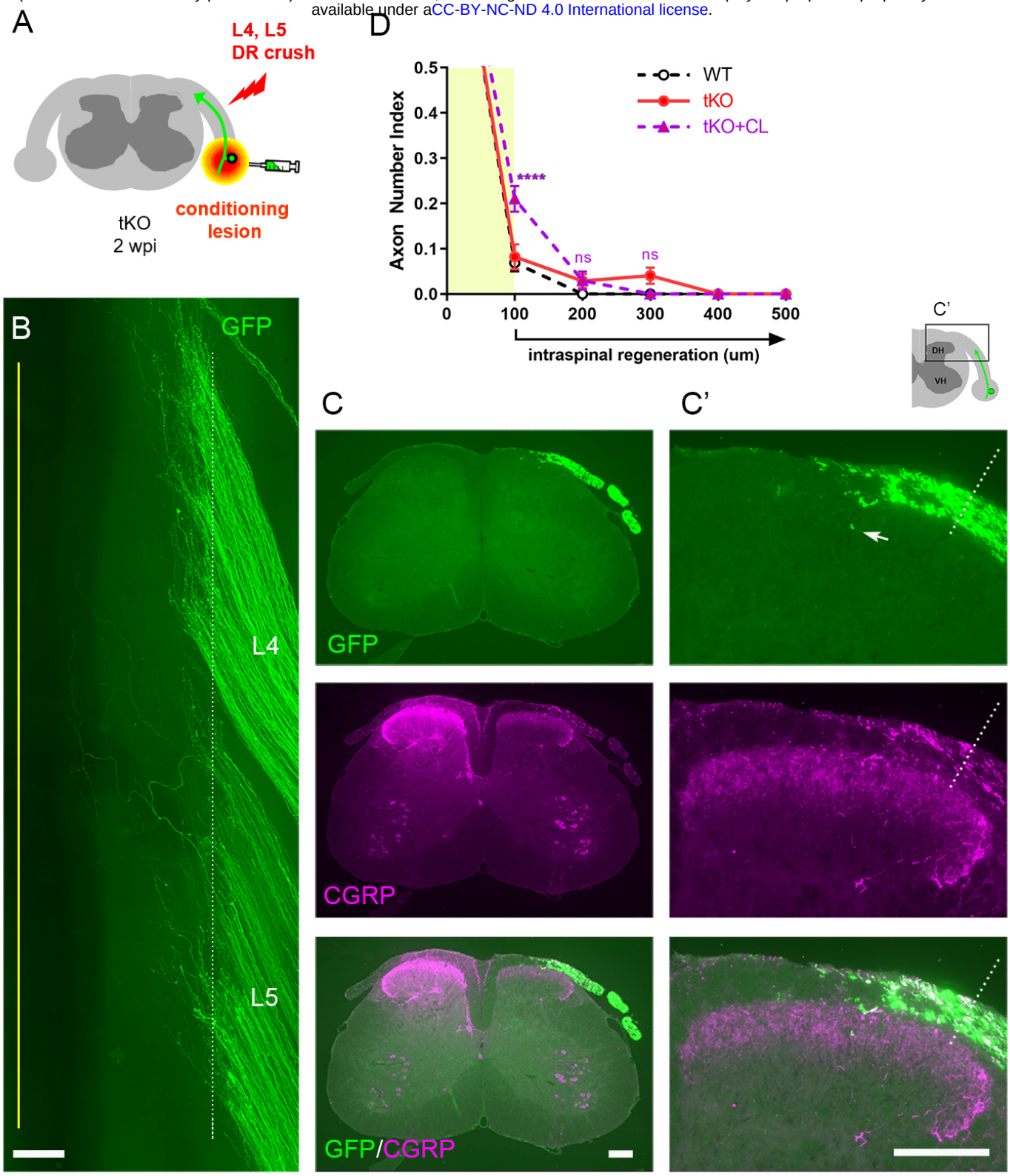

Figure 6. Conditioned DR axons do not penetrate the DREZ lacking Nogo/MAG/OMgp

(A) Schematic illustration of the experimental procedures. Nogo/MAG/OMgp tKO mice received a nerve conditioning lesion 10 days before L4 and L5 DR crush and were assessed at 2wpi. **(B)** Wholemount view of a conditioned tKO showing hundreds of GFP+ axons terminated near the astrocyte:PNS border (dotted line), as in WT and tKO mice. **(C, C')** Transverse sections of a conditioned tKO illustrating little if any enhanced regeneration of GFP+ (green) or CGRP+ axons (magenta) across the DREZ. An arrow denotes occasionally observed GFP+ axons that reached dorsolateral grey matter. **(D)** Quantitative comparisons illustrating no significant difference in WT, tKO and conditioned tKO mice. tKO vs. conditioned tKO: 100µm, ****$p < 0.0001$, df=220; 200µm, $p = 0.9991$, df=220; 300µm, $p > 0.9999$, df=220. Two-way repeated-measures ANOVA with Sidak's multiple comparisons test (WT: 13 sections, 3 mice; tKO: 16 sections, 5 mice; conditioned-tKO: 11 sections, 3 mice). ns, not significant. Scale bars=200µm (**B, C, C'**).

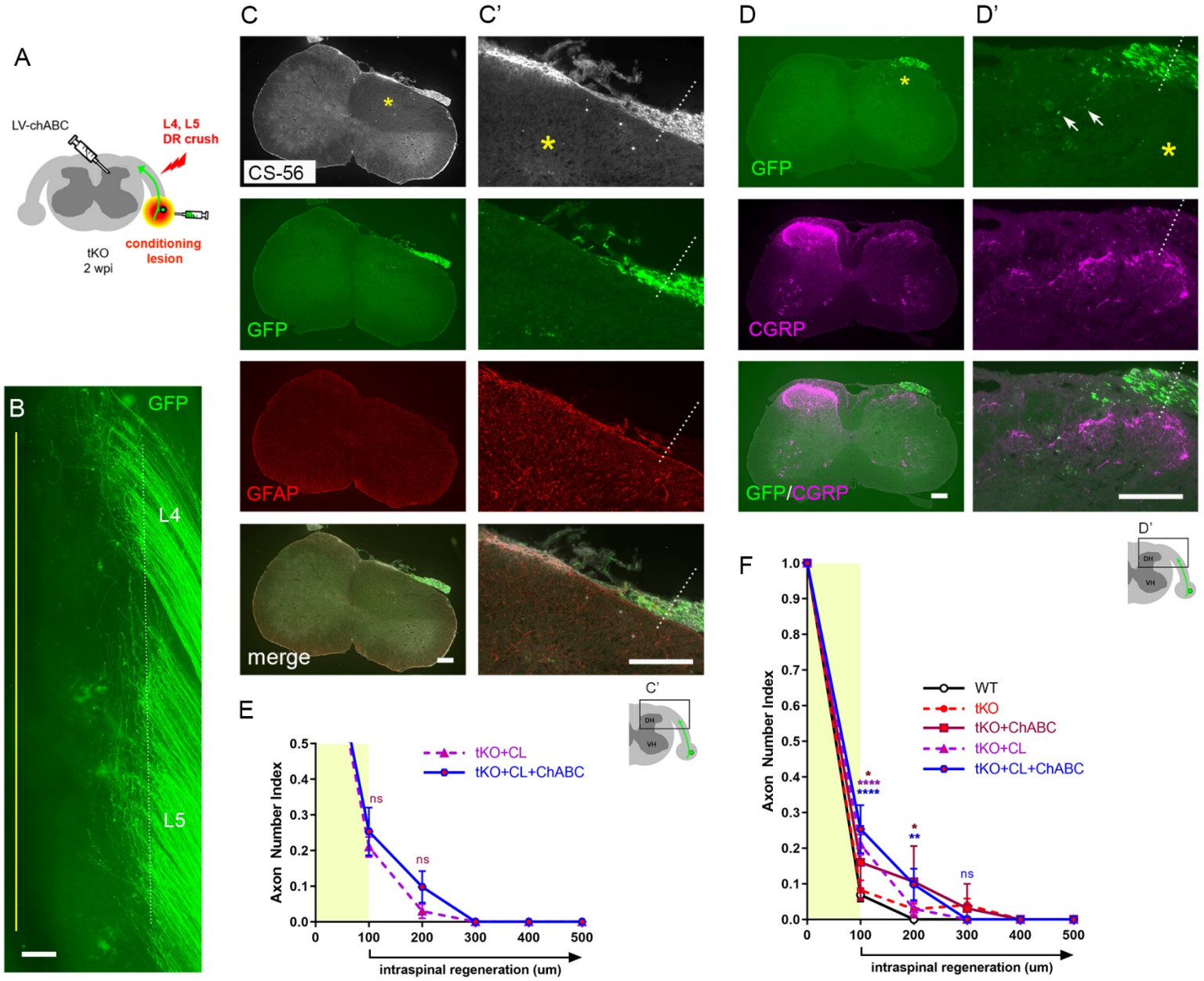

Figure 7. Additional CSPG removal does not enhance penetration in conditioned tKO mice
(A) Schematic illustration of the experimental procedures. LV-ChABC was injected into Nogo/MAG/OMgp tKO mice that received a conditioning lesion 10 days before L4 and L5 DR crush. **(B)** Wholemount view of a ChABC/conditioned tKO showing hundreds of GFP+ axons that remain near the border (dotted line). **(C-C')** Transverse sections of a ChABC/conditioned tKO illustrating effective CSPG degradation confirmed by the lack of CS-56 immunoreactivity (asterisks) and little if any intraspinal regeneration of GFP+ axons. **(D-D')** Additional transverse sections of a ChABC/conditioned tKO illustrating limited intraspinal regeneration of GFP+ or CGRP+ axons (magenta). Arrows denote occasionally observed GFP+ axons that enter dorsal grey matter. **(E)** Quantitative comparisons illustrating no significant difference in ChABC/conditioned tKO and conditioned tKO mice. 100µm, p=0.7629, df=114; 200µm, p=0. 2671, df=114. Two-way repeated-measures ANOVA with Sidak's multiple comparisons test (conditioned tKO: 11 sections, 3 mice; ChABC/conditioned tKO: 10 sections, 4 mice). **(F)** Quantitative summary illustrating minimal intraspinal regeneration of even conditioned axons after concurrent removal of myelin inhibitors and CSPGs; Only ~10% GFP+ axons extended ~100um past the DREZ. 100µm, *p=0.0488, df=300 (WT vs ChABC expressed tKO), ****p<0.0001, df=300 (WT vs conditioned tKO, WT vs ChABC/conditioned tKO); 200µm, *p=0.014, df = 300 (WT vs ChABC expressed tKO, **p=0.0024, df = 300 (WT vs ChABC/conditioned tKO); 300 µm, p>0.9999; df = 300. Two-way repeated-measures ANOVA with Sidak's multiple comparisons test. Scale bars=200µm (**B, C, C', D, D'**).

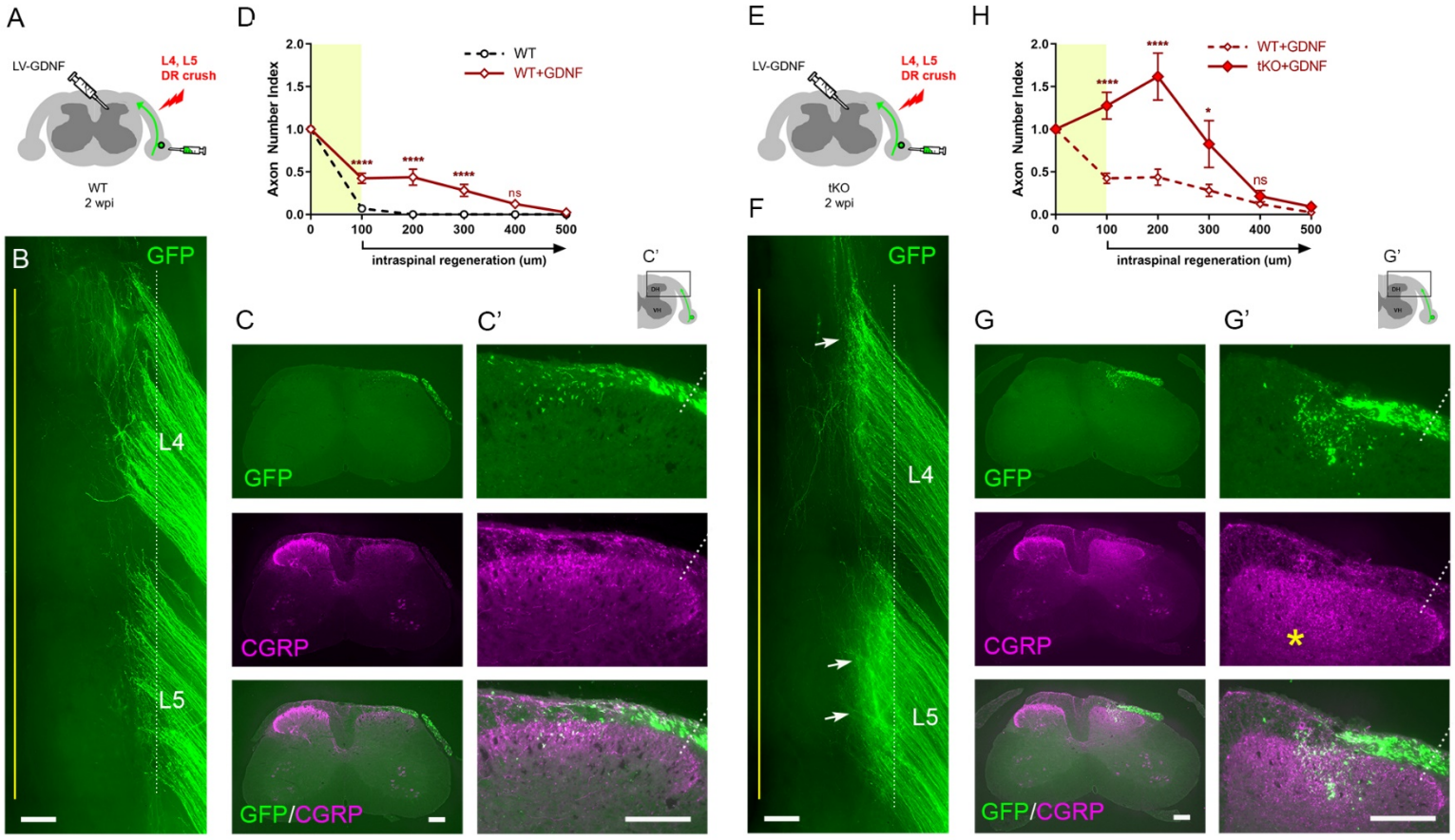

Figure 8. Nogo/MAG/OMgp removal markedly enhances GDNF-induced intraspinal regeneration
GDNF-induced intraspinal regeneration analyzed in WT (**A-D**) and Nogo/MAG/OMgp tKO mice (**E-G'**) 2 weeks after L4 and L5 DR crush. **(A)** Schematic illustration showing intraspinal injections of LV-GDNF at the time of root crush and AAV2-GFP injections in WT mice. **(B)** Wholemount view of a GDNF-expressed WT illustrating hundreds of GFP+ axons largely remaining near the border. **(C-C')** Transverse sections of a GDNF-expressed WT showing a number of GFP+ (green) or CGRP+ axons (magenta) that cross the DREZ and extend further into the dorsal funiculus and grey matter. **(D)** Quantitative comparisons illustrating significantly enhanced penetration of GFP+ axons across the DREZ. 100µm, 200µm and 300µm, ****p<0.0001, df=156; 400µm, p=0.2446, df=156. Two-way repeated-measures ANOVA with Sidak's multiple comparisons test (WT: 13 sections, 3 mice; GDNF-expressed WT: 15 sections, 3 mice). **(E)** Schematic illustration of the experimental procedures in Nogo/MAG/OMgp tKO mice. **(F)** Wholemount view of a GDNF-expressed tKO mouse revealing intensely fluorescent area of the L4 and L5 DREZ (arrows), likely due to densely accumulated subdural GFP+ axons. **(G-G')** Transverse sections of a GDNF-expressed tKO mouse displaying numerous GFP+ axons regenerating deep into dorsal horn. Asterisks denote CGRP immunoreactivity in deep dorsal laminae (magenta), presumably indicating enhanced regeneration of CGRP+ axons in GDNF-expressed tKO, as compared to that in GDNF-expressed WT. **(H)** Quantitative comparisons illustrating markedly greater intraspinal growth of GFAP-labeled axons in GDNF-expressed tKO than in GDNF-expressed WT mice. 100µm and 200µm, ****p<0.0001, df=174; 300µm, *p=0.028, df=174; 400µm, p=0.9975, df=174. Two-way repeated-measures ANOVA with Sidak's multiple comparisons test (GDNF-expressed WT: 15 sections, 3 mice; GDNF-expressed tKO: 16 sections, 5 mice). ns, not significant. Scale bars=200µm (**B, C, C', F, G, G'**).

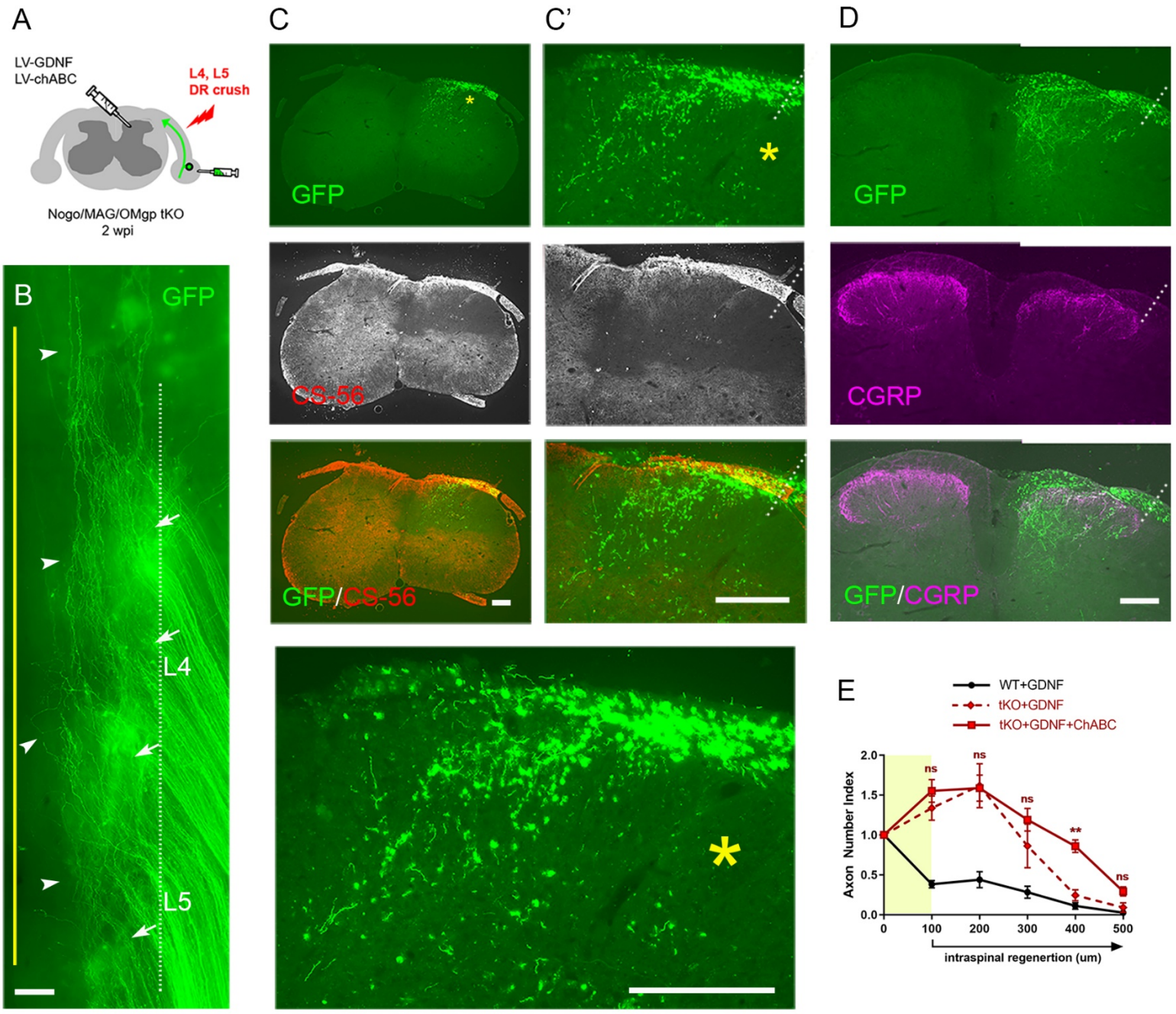

Figure 9. CSPG removal further enhances GDNF-induced intraspinal regeneration in Nogo/MAG/OMgp tKO mice

(A) Schematic illustration of the experimental procedures. LV-ChABC and LV-GDNF were injected into dorsal horn along the L4-L5 DREZ in Nogo/MAG/OMgp tKO mice. **(B)** Wholemount view of a ChABC/GDNF-expressed tKO showing broader areas of the DREZ and the CNS with densely accumulated GFP+ axons (arrows). Arrowheads denote numerous axons extending rostrocaudally close to the midline. **(C-C')** Transverse sections of a ChABC/GDNF-expressed tKO showing effective degradation of CSPGs confirmed by CS-56 immunoreactivity and many GFP+ axons densely filling broad and deep areas of the dorsal horn. **(D)** Transverse sections of a ChABC/GDNF-expressed tKO showing enhanced intraspinal regeneration of GFP+ axons and CGRP+ axons (magenta). CGRP+ immunoreactivity is bright, dense and remarkably restricted to the superficial laminae. **(E)** Quantitative comparisons illustrating significantly more GFP+ axons in deeper portions of the dorsal horn in ChABC/GDNF-expressed tKO. 100μm, p=0.5389, df=210; 200μm, p=0.9891, df=210; 300μm, p=0.2358, df=210; 400μm, p=0.0074, df=210; 500μm, p=0.5805, df=210. Two-way repeated-measures ANOVA with Sidak's multiple comparisons test (ChABC/GDNF-expressed tKO: 19 sections, 8 mice; GDNF-expressed tKO: 16 sections, 5 mice). ns, not significant. Scale bars=200μm **(B, C, C', D)**.